August 2019

An Application of Conformal Mapping to the Boundary Element Method for Unconfined Steady Seepage with a Phreatic Surface

Jorge Eduardo Reyes
reyesj1@unlv.nevada.edu

AN APPLICATION OF CONFORMAL MAPPING TO THE BOUNDARY ELEMENT

METHOD FOR UNCONFINED STEADY SEEPAGE WITH

A PHREATIC SURFACE

By

Jorge Reyes

Bachelor of Science - Mathematics
University of Nevada, Las Vegas
2015

A thesis submitted in partial fulfillment
of the requirements for the

Master of Science - Mathematical Sciences

Department of Mathematical Sciences
College of Sciences
The Graduate College

University of Nevada, Las Vegas
August 2019

Thesis Approval

The Graduate College
The University of Nevada, Las Vegas

August 5, 2019

This thesis prepared by

Jorge Reyes

entitled

An Application of Conformal Mapping to the Boundary Element Method for Unconfined Steady Seepage with a Phreatic Surface

is approved in partial fulfillment of the requirements for the degree of

Master of Science - Mathematical Sciences
Department of Mathematical Sciences

Angel Muleshkov, Ph.D.   Kathryn Hausbeck Korgan, Ph.D.
Examination Committee Chair   *Graduate College Dean*

Monika Neda, Ph.D.
Examination Committee Member

Pengtao Sun, Ph.D.
Examination Committee Member

David Kreamer, Ph.D.
Graduate College Faculty Representative

ABSTRACT

An Application of Conformal Mapping to the Boundary Element Method for

Unconfined Steady Seepage with a Phreatic Surface

By

Jorge Reyes

Dr. Angel Muleshkov, Examination Committee Chair
Associate Professor of Mathematical Sciences
University of Nevada, Las Vegas

In this thesis, numerical results using the Boundary Element Method (BEM) for groundwater flow in a domain with a boundary that contains numerous singularities with a phreatic surface are developed. The flow in the domain is modeled using Darcy's law for a homogeneous isotropic porous medium. The boundary conditions are a combination of Dirichlet and Neumann with the phreatic surface having both boundary conditions. Exact solutions by Conformal Mapping for simplified domains with the same singularity as the original domain allow for modifications to the BEM resulting in an improvement to the numerical solution.

An iterative process is used to determine the location of the phreatic surface and the location of the exit point. The iteration starts with an initial guess for the phreatic surface using the exact solution by conformal mapping for an infinite unconfined domain that preserves the important features of the domain around phreatic surface near the exit point.

Initially, the problem is solved using the conventional BEM as described by Liggett and Liu (1983). It is expected that the singularities and unknown location of the phreatic surface will lead

iii

to a failure of the BEM solution especially near the singular points and on the phreatic surface. Then, the modified BEM with the conformal mapping improvements is used to find the solution. The modified and conventional BEM are then compared with an emphasis on accuracy of the numerical solutions. Several tables and figures are produced to illustrate the results.

ACKNOWLEDGEMENTS

DEDICATION

I dedicate this thesis to my son, Jorge Eduardo Reyes III. I hope some day you read this and it sparks some kind of conversation about math or life. I love you, and know that everything I do, I do for you. You truly motivate me to be the best version of myself and I hope someday you are proud of your dad and his accomplishments.

I also wish to dedicate this to my parents. You have sacrificed so much me and given me all the love and support I could ever ask for. Te quiero mucho y si tengo suerte puedo agradecerte otra vez en mi disertacion.

TABLE OF CONTENTS

LIST OF FIGURES

CHAPTER 1

INTRODUCTION

1.1 Groundwater Flow and Darcy's Law

The dynamics of fluids in a porous media have long been studied. It is a subject of interest for Groundwater Hydrology as well as many fields of Physics and Engineering. The following work is based on the assumptions that allow the use of Darcy's Law which establishes linear dependency between the discharge velocity and the hydraulic gradient given in Eq.(1.5) (Harr, 1962; Bear, 1972; 2018).

The conditions in which Darcy's Law can be used to model a flow are as follows. The first assumption in Darcy's Law is that the flow is steady, specifically laminar, which is found at lower velocities (Harr, 1962; Bear, 1972; 2018). This, however, raises the question about where exactly does laminar flow end and turbulent flow begin. In what is an oversimplification to the actual answer, it seems that having a Reynolds' number less than 1 seems to distinguish laminar flow and where Darcy's Law seems to be valid, although sometimes a Reynolds' number as high as 10 can work (Bear, 2018; Harr, 1962).

The following additional conditions are imposed for the purposes of allowing Darcy's Law to be described with the two-dimensional Laplace equation. The soil is assumed homogeneous and isotropic, the fluid is incompressible, and the flow has the same movement in vertical parallel planes.

The formulation of Darcy's Law typically begins with the following Bernoulli equation (Harr, 1962)

$$H = \frac{p}{\rho g} + z + \frac{v^2}{2g}. \tag{1.1}$$

Where

H is Total Hydraulic head

$\frac{p}{\rho g}$ is the pressure head

z is the elevation head

$\frac{v^2}{2g}$ is the velocity head

p is the atmospheric pressure

ρ is the density of the fluid

g gravitational constant

Eq.(1.1) shows that the sum of the pressure head, elevation head, and velocity head at any point in a domain is constant (Harr, 1962). If we take $v \ll 1$ since groundwater flow is exceptionally slow, the velocity head can be neglected and Eq.(1.1) becomes

$$h = \frac{p}{\rho g} + z \tag{1.2}$$

where h is now considered the piezometric head (Bear, 2018; Harr, 1962; Liggett and Liu, 1983).

We now begin with the Navier-Stokes equation for incompressible flow

$$\begin{cases} \rho \left(\dfrac{\partial v}{\partial t} + v \cdot \nabla v \right) = \Delta v - \nabla h + f \\[2ex] \nabla \cdot v = 0 \end{cases} \tag{1.3}$$

where v is the velocity, and f is an external force (Tice, 2014; Layton, 2008; Bear, 2018). The fact that we assume that the seepage is steady allows us to neglect the term regarding time (Tice, 2014). Since we have also assumed a sufficiently low Reynolds number, the $v \cdot \nabla v$ term drops out

2

of the equation as well (Layton, 2008), and thus Eq.(1.3) becomes the Stokes equation

$$
\begin{cases}
-\Delta v + \nabla h = f \\[2mm]
\nabla \cdot v = 0
\end{cases}
\tag{1.4}
$$

(Tice, 2014; Layton, 2008; Bear, 1972; 2018). The homogeneous and isotropic conditions then allow Eq.(1.4) to become

$$
v = K \left(f - \nabla h \right)
\tag{1.5}
$$

Where K is the coefficient of permeability which in this case is a constant. Eq.(1.5) is commonly referred to as Darcy's Law (Tice, 2014; Bear, 1972; 2018; Harr, 1962; Bruch, 1991). In our case there are no external forces such as sinks or sources so $f = 0$ and Eq.(1.5) becomes

$$
v = -K\nabla h
\tag{1.6}
$$

and we now clearly see that the discharge velocity is linearly dependent on the hydraulic gradient (Harr, 1962; Bear, 1972).

Now, If we apply the Law of Conservation of Mass to Eq.(1.6), we get

$$
\operatorname{div}(K\nabla h) = 0 \implies \Delta h = 0
\tag{1.7}
$$

which is the two-dimensional Laplace equation written as

$$
\frac{\partial^2 h}{\partial x^2} + \frac{\partial^2 h}{\partial y^2} = 0.
\tag{1.8}
$$

"It is of the utmost convenience in groundwater flow to introduce the *velocity potential* ϕ, defined

3

as

$$\phi = -Kh + C \tag{1.9}$$

where C is an arbitrary constant"(Harr, 1962). From Eq.(1.9) and Eq.(1.8) it is clear that we also

have

$$\frac{\partial^2 \phi}{\partial x^2} + \frac{\partial^2 \phi}{\partial y^2} = 0. \tag{1.10}$$

Therefore, both h and ϕ are harmonic functions, and groundwater flow can be modeled by the

two-dimensional Laplace equation (Harr, 1962; Bruch, 1991; Chantasiriwan, 2011; Cedergen, 1968;

Bear, 1972; 2018; Muleshkov, 1988).

1.2   Solving Two-Dimensional Laplace Boundary Value Problems

The methods discussed in this section will be limited to those deemed relevant for the type of

domains with boundary conditions as in this thesis. The boundary conditions used in this thesis

are Dirichlet, and zero Neumann (Evans, 2010).

The Two-Dimensional Laplace equation has a rich history of being solved using conformal

mapping. A conformal mapping is a function $f(z)$ that is said to preserve local angles (Mathews and

Howell, 2012). Using this fact in concert with potential theory, the theory of harmonic functions,

and the Riemann Mapping Theorem gives mathematicians and engineers a powerful tool for solving

the two-dimensional Laplace equation (Muleshkov, 2016). The conformal mapping $f(z) = u(x, y) +$

$iv(x, y)$ solves boundary value problems (BVPs) if $f(z)$ maps D onto D^*, is one-to-one, analytic

at every point in D, and $f'(z_0) \neq 0$ for every point z_0 in D (Mathews and Howell, 2012; Carrier

et al., 1983). This mapping's existence and uniqueness can be proven with the Riemann Mapping

Theorem, but it does not give a procedure for finding the conformal mapping (Carrier et al., 1983;

Muleshkov, 2016). The details on how we find our conformal mappings are given in section 2.3.

Numerical methods that can solve BVPs for the two-dimensional Laplace equation are in no short supply. The Finite Element Method (FEM), is currently a popular method used by many fields of Engineering and Physics. This thesis focuses on the Boundary Element Method (BEM), a popular alternative to FEM depending on the specifics of the problem. Other methods include finite difference methods (FDM), meshless methods, mixed methods, and many others.

1.3   Previous Work on BEM Solutions with Singularities and Phreatic Surfaces.

1.3.1   BEM Solutions with Singularities on the Boundary

The BEM is well established among engineering circles. As such, there are many articles and resources on using the BEM under a wide variety of situations. In this brief overview, we focus on work related to this thesis, particularly, on how others dealt with singularities on the boundary while using the BEM.

Traditionally, when using the BEM, the boundary is discretized into elements, small portions of the boundary (usually line segments), with nodes connecting them. On the elements with Dirichlet boundary conditions, where ϕ is given, $\dfrac{\partial \phi}{\partial n}$ will be linearly approximated using linear interpolation between the two nodes at the end of the elements, where the normal derivative is unknown and desired. Similarly, the elements with Neumann boundary conditions, where $\dfrac{\partial \phi}{\partial n}$ is given, ϕ will be linearly approximated using linear interpolation between the two nodes at the end of the element where the value of the function is unknown and desired.

When there are singularities on the boundary, the previous methodology may need to be adjusted. For instance, some books elect to use higher order interpolations on the elements adjacent to the singularities (Kythe, 1995). This may help the method get better results, though it does not

5

get to the heart of the issue.

A different approach would be to ignore the singularities by using discontinuous elements around the singularity. This is done since $\dfrac{\partial \phi}{\partial n}$ does not exist at the corner where the singularity is. Instead of having one node at the corner, two nodes are placed on ether side of the corner, for instance, at a distance of ε and δ away (Kythe, 1995; Bruch, 1991). This method will be used as the "traditional method" when finding the BEM solution in this thesis.

Another method that has been used is to subtract a solution of the function ϕ around the singularity (Igarashi and Honma, 1996; Lefeber, 1989). This method is based on the regularized function method in which a regularized function $\psi(x)$ is introduced in place of the potential function $\phi(x)$, where $\phi(x) = \phi_k + \displaystyle\sum_{l=1}^{\infty} a_{kl}\hat{g}_{kl}(x)$ and $\hat{g}_{kl}(x)$ is a special solution about the singular point. $\psi(x)$ is now set as $\phi(x) - \displaystyle\sum_{k=1}^{K}\sum_{l=1}^{L} a_{kl}\hat{g}_{kl}(x)$ and Igarashi and Honma now note that $\psi(x)$ "no longer possesses singularity, since the singular term ... have been subtracted off from ϕ" (Igarashi and Honma, 1996). Then the BEM is used and once the coefficient(s) of the special solution(s) about the singularities are found, ϕ can be found.

The last method discussed is introduced by Muleshkov (1988). This method alters the interpolation used around the singularity to find the unknown variable $\left(\phi \text{ or } \dfrac{\partial \phi}{\partial n}\right)$, but not by just using an interpolation of a higher order. The function used is obtained from a conformal mapping solution of a similar domain where the sides of the singularity are extended infinitely. The boundary conditions are preserved as to get the correct local behavior around the singularity. The fact that the exact conformal mapping solution is imposed on the elements adjacent to the singularity leads to an improvement of the BEM in terms of accuracy around the singularity and inside the domain itself.

This Thesis focuses on the method developed by Muleshkov (1988). Megan Romero's (2018)

6

thesis took a further look into the this method by comparing the traditional method to the modified method with the exact solution in a rectangle and another generalized polygon. In this thesis, we further expand on the work of Romero by looking at a domain containing the arc of a circle, but more importantly a domain with a phreatic surface. A phreatic surface is also often called a free surface in modern literature and is often used when modeling two-dimensional unconfined flow. The inclusion of a phreatic surface often causes difficulties since a portion of the boundary is unknown and the location of a phreatic surface deserves its own research that is discussed in the following subsection.

1.3.2   Locating the Phreatic Surface

Regardless of the methods chosen the solve the BVP (FDM, FEM, BEM) the most common way of locating a phreatic surface is some kind of iteration (Chen et al., 2007). For FDM and FEM what is frequently employed is some kind of adaptive mesh (Lacy and Prevost, 1987; Yeung, 1982; Wang et al., 2015). Nevertheless, "Free-surface flows seem particularly suitable for integral-equation treatment since physical quantities of primary interest ... are required only on the boundaries." (Yeung, 1982). This is the one of the primary reasons the BEM was chosen over the other numerical methods. This thesis uses the algorithm outlined in Chantasiriwan (2011) for finding the location of the exit point, or to the same effect, finding the width of the seepage surface. The iterative procedure used is taken from Burch (1991). The initial guess is derived in a similar way to what is done in Muleshkov (1988) with just slight changes. The results and possible further research will be given in Chapter 5.

<center>CHAPTER 2</center>

<center>BACKGROUND KNOWLEDGE AND INTRODUCTION OF THE</center>

<center>PROBLEM</center>

2.1   Domain and Boundary Conditions of the Problem

In this thesis we will solve the Laplace equation BVP for a domain that is chosen sufficiently complicated as to allow realistic modeling of groundwater flow. The seepage problem that we solve using the BEM and the modified BEM has the following boundary conditions:

On AB, $\phi(x, 0) = 0$, $0 < x < b$

On BC, $\phi(x, g(x)) = g(x) \ \wedge \ \dfrac{\partial \phi}{\partial n}(x, g(x)) = 0$, $-\ell_1 < x < b$

On CD, $\phi(-\ell_1, y) = \ell_3$, $d < y < \ell_3$

On DE, $\phi(x, -x - \ell_2 - 2R) = \ell_3$, $-\ell_1 < x < -R$

On EF, $\dfrac{\partial \phi}{\partial n}(R \cos \theta, R \sin \theta - \ell_2 - R) = 0$, $\dfrac{\pi}{2} < \theta < \pi$

On FA, $\dfrac{\partial \phi}{\partial n}(0, y) = 0$ $-\ell_2 < y < 0$

Which results in Figure 2.1. Note $\kappa = -\ell_2 - R$.

We may observe that points A, D, E, F are all singularities. Point B's (the exit point) x-coordinate is unknown, and the shape and location of the phreatic surface, $g(x)$, is unknown. Note that points B and C are regular points since they are an intersection of a streamline and an equipotential line with the angle formed at the point being $\dfrac{\pi}{2}$.

<center>8</center>
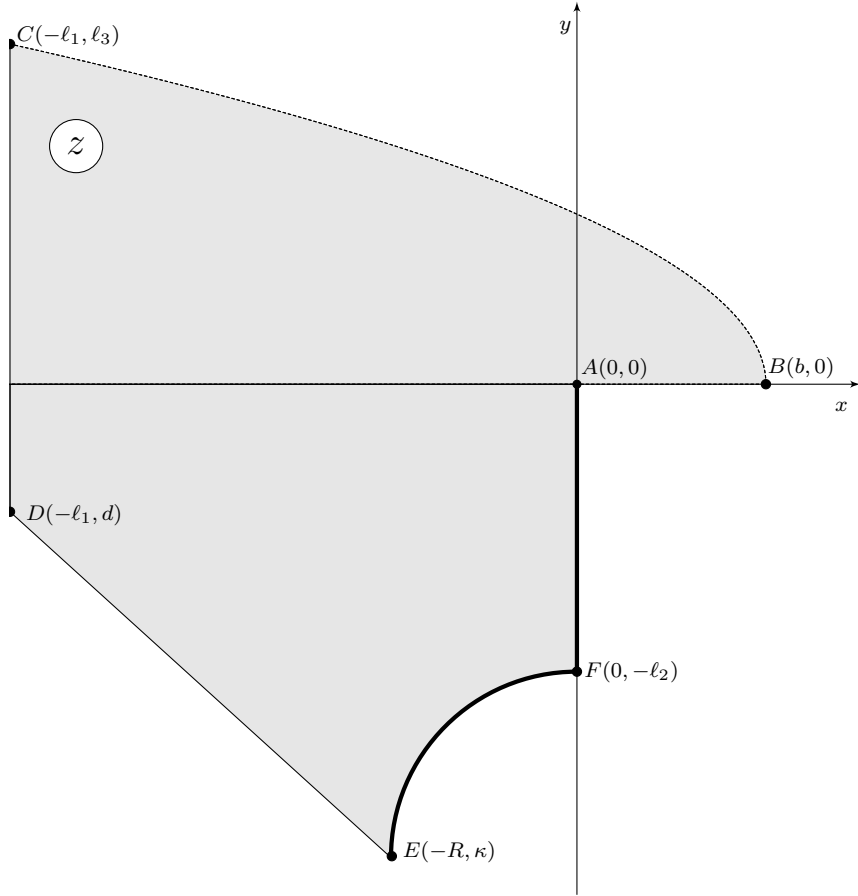
Figure 2.1: Physical Domain/Domain of Interest, z-plane.

2.2   The Boundary Element Method

This section introduces some of the basic theory of BEM within the context applicable to the problems in this thesis. Given twice differentiable functions $U(x,y)$ and $V(x,y)$, in a domain, D , we apply Green's Second Identity,

$$\iint_D \left(U\nabla^2 V - V\nabla^2 U\right) dxdy = \oint_{\partial D} \left(U\frac{\partial V}{\partial n} - V\frac{\partial U}{\partial n}\right) ds, \tag{2.1}$$

where $\dfrac{\partial U}{\partial n}$ and $\dfrac{\partial V}{\partial n}$ are the normal derivatives of $U(x,y)$ and $V(x,y)$, respectively. If $U(x,y)$ and $V(x,y)$ are harmonic, then $\nabla^2 U = 0$ and $\nabla^2 V = 0$, hence Eq.(2.1) becomes equation

$$0 = \oint_{\partial D} \left(U \frac{\partial V}{\partial n} - V \frac{\partial U}{\partial n} \right) ds. \tag{2.2}$$

$U(x,y)$ and $V(x,y)$ can then be chosen to be:

$$U(x,y) = \phi(x,y), \qquad V(x,y) = \ln r_p$$

Where $V(x,y)$ can be obtained from the Fundamental Solution for the two-dimensional Laplace equation and $r_p = \sqrt{(x - x_p)^2 + (y - y_p)^2}$ is the distance from the point (x,y) to a fixed point P, (x_p, y_p). Plugging in our chosen functions for $U(x,y)$ and $V(x,y)$ Eq.(2.2) becomes

$$\oint_{\partial D} \left(\frac{\phi}{r_p} \frac{\partial r_p}{\partial n} - \frac{\partial \phi}{\partial n} \ln r_p \right) ds = 0. \tag{2.3}$$

If $(x_p, y_p) = (x, y)$, then $r_p = 0$ which causes a singularity of the integrand in Eq.(2.3) (Liggett and Liu, 1983; Muleshkov, 1988). To remedy this problem, we evaluate Eq. (2.3) with its principal value, giving us

$$\text{p.v.} \oint_{\partial D} \left(\frac{\phi}{r_p} \frac{\partial r_p}{\partial n} - \frac{\partial \phi}{\partial n} \ln r_p \right) ds = \alpha_p \phi_p \tag{2.4}$$

where α_p is the angle that is formed by the adjacent segments of point P (Liggett and Liu, 1983). If point P is on a smooth part of the boundary, then the angle is π. Whereas if point P is inside the boundary, then the angle is 2π.

In this case, since the boundary of D is discretized into segments with nodes at the endpoints $s = s_m$ and $s = s_{m+1}$, Eq.(2.4) becomes

10

$$\int_{s_m}^{s_{m+1}} \left(\frac{\phi}{r_p} \frac{\partial r_p}{\partial n} - \frac{\partial \phi}{\partial n} \ln r_p \right) ds + \int_{s_{m+1}}^{s_{m+2}} \left(\frac{\phi}{r_p} \frac{\partial r_p}{\partial n} - \frac{\partial \phi}{\partial n} \ln r_p \right) ds + \cdots = \alpha_p \phi_p \qquad (2.5)$$

where m and p go from 0 to $N-1$. Eq.(2.5) can be written in the more compact form

$$\sum_{p=0}^{N-1} \sum_{m=0}^{N-1} I_{m,m+1}^{(p)} = \alpha_p \phi_p \qquad (2.6)$$

where

$$I_{m,m+1}^{(p)} = \int_{s_m}^{s_{m+1}} \left(\frac{\phi}{r_p} \frac{\partial r_p}{\partial n} - \frac{\partial \phi}{\partial n} \ln r_p \right) ds. \qquad (2.7)$$

As previously mentioned, ϕ or $\frac{\partial \phi}{\partial n}$ will be linearly approximated depending on which is unknown. This unknown value will be denoted by Ω, where Ω_m represents ϕ or $\frac{\partial \phi}{\partial n}$(whichever is unknown) at the mth point/node. Using the endpoint nodes s_m and s_{m+1} we can get the following linear interpolation

$$\Omega = \Omega_m \left(\frac{s_{m+1} - s}{s_{m+1} - s_m} \right) + \Omega_{m+1} \left(\frac{s - s_m}{s_{m+1} - s_m} \right). \qquad (2.8)$$

Pugging in Eq.(2.8) into Eq.(2.7), one gets

$$I_{m,m+1}^p = \Omega_m \cdot a_{p,m}^{(m)} + \Omega_{m+1} \cdot a_{p,m+1}^{(m)} + B_{p,m} \qquad (2.9)$$

where $a_{p,m}^{(m)}$ and $a_{p,m+1}^{(m)}$ are the coefficients of Ω_m and Ω_{m+1}, respectively, and $B_{p,m}$ is the evaluated integral that contains the known constant from the boundary conditions.

Similarly, if we have endpoints s_{m-1} and s_m in Eq.(2.7), we arrive at the following equation

$$I_{m-1,m}^p = \Omega_{m-1} \cdot a_{p,m-1}^{(m-1)} + \Omega_m \cdot a_{p,m}^{(m-1)} + B_{p,m-1}. \qquad (2.10)$$

11

Now we can define $A_{p,m}$ as the coefficient of Ω_m using Eqs.(2.9),and (2.10) as

$$A_{p,m} = a_{p,m}^{(m-1)} + a_{p,m}^{(m)} - \delta_p \alpha_p \phi_p \tag{2.11}$$

where $\delta_p = \begin{cases} 1, & \phi_p \text{ is unknown} \\ \\ 0, & \phi_p \text{ is known} \end{cases}$,

and the integral that results from ϕ or $\dfrac{\partial \phi}{\partial n}$ being known on an element can be written as

$$B_p = \alpha_p(1 - \delta_p)\phi_p - \sum_{m=0}^{N-1} B_{p,m} \tag{2.12}$$

where p goes from 0 to $N - 1$ (Muleshkov, 1988).

We can then use Eqs.(2.15) and (2.12) to form a system of linear equations,

$$\sum_{m=0}^{N-1} A_{p,m}\Omega_m = B_p \tag{2.13}$$

where p goes from 0 to $N - 1$ (Muleshkov, 1988).

In matrix form, Eq.(2.13) can be written as

$$[A]_{N,N}[\Omega]_{N,1} = [B]_{N,1}. \tag{2.14}$$

Later on, once the right hand side of Eq.(2.9) is evaluated, we know $a_{p,m}^{(m)}$ in the form of an integral that depends on the the portion of the boundary being evaluated I.

$$a_{p,m}^{(m)} = I(x_m, x_{m+1}, y_m, y_{m+1}, \dots). \tag{2.15}$$

This is further discussed in Chapter 3 and 4. Once $a_{p,m}^{(m)}$ is known, then $a_{p,m}^{(m-1)}$ can be conveniently found by the following formula

$$a_{p,m}^{(m-1)} = -I(x_m, x_{m-1}, y_m, y_{m-1}, \dots)$$ (2.16)

(Muleshkov, 1988).

2.3   A Simplified Domain with Similar Toe Drain and Phreatic Surface

The Boundary Conditions on all domains discussed will have a combination of Dirichlet and Neumann with the phreatic surface having both boundary conditions. It should be noted that the Neumann boundary condition will always be zero, which in turn allows us to use conformal mapping in the problem. The domain in Figure 2.2 has the following boundary conditions:

On AB, $\varphi(x, 0) = 0, \quad 0 < x < b$

On BC, $\varphi(x, h(x)) = y \ \wedge \ \dfrac{\partial \varphi}{\partial n}(x, h(x)) = 0, \quad x < b$

On CA, $\dfrac{\partial \varphi}{\partial n}(0, y) = 0 , \quad y < 0.$

Figure 2.2 is simple enough to allow us to solve the Laplace BVP analytically using conformal mapping, which is done in Sec 2.4, yet with proper assumptions still similar enough to Figure 2.1 to allow us to use the results as the initial guess for the shape and location of the phreatic surface $h(x)$ for the iteration.
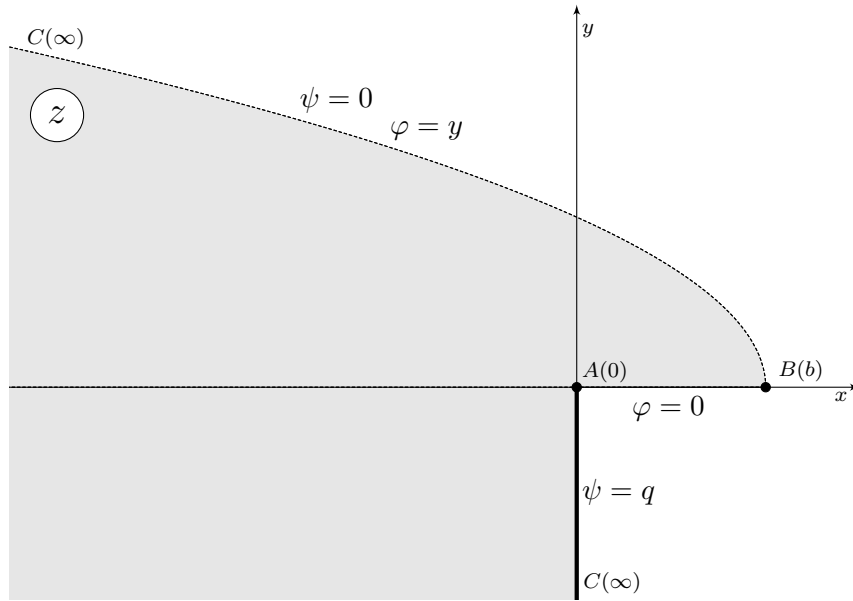
Figure 2.2: Simplified Domain, z-plane.

We may observe that point A is a singularity since the angle formed at point A is $\dfrac{3\pi}{2}$, Point B's (the exit point) x-coordinate is unknown, on CA ψ equals a constant q, and the shape and location of the phreatic surface, $h(x)$, is unknown.

Now, examining the boundary conditions, we can divine that the corresponding domain in the complex potential plane looks like the domain in Figure 2.3
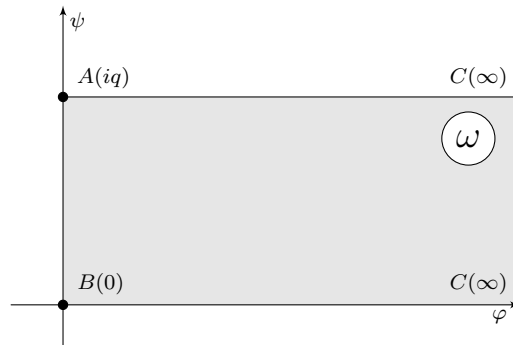
Figure 2.3: Domain in Complex Potential Plane, ω-plane

14

2.4 Exact Conformal Mapping Solution for the Simplified Domain

The immediate difficulty when dealing with a phreatic surface is the fact that the shape and location are unknown. We are in turn compensated by having two boundary conditions on the phreatic surface, one for the function and one for the normal derivative. Nevertheless, finding a conformal mapping from the physical domain in the z-plane to its image in the ω-plane , where $\omega = \varphi + i\psi$ is the complex potential, is impossible. This problem is remedied by the use of an auxiliary function $W(\omega) = \dfrac{\mathrm{d}z}{\mathrm{d}\omega}$, which is the reciprocal of the complex velocity or the Kirchoff function (Harr, 1962; Carrier et al., 1983). This process will now be shown with the domain in Figure 2.2. Let $u = \mathrm{Re}[W]$ and $v = \mathrm{Im}[W]$.

On AB, $\varphi = 0 \wedge y = 0 \implies z = x \wedge \omega = i\psi$. Thus,

$$W = \frac{\mathrm{d}z}{\mathrm{d}\omega} = \frac{\mathrm{d}x}{i\mathrm{d}\psi} = -i\frac{\mathrm{d}x}{\mathrm{d}\psi} \tag{2.17}$$

where $u = 0$ and $v = -\dfrac{\mathrm{d}x}{\mathrm{d}\psi}$. Since $\mathrm{d}x > 0$ and $\mathrm{d}\psi < 0$ then $v > 0$.

On BC, $\varphi = y \wedge \psi = 0 \implies z = x + iy \wedge \omega = y$. Thus,

$$W = \frac{\mathrm{d}z}{\mathrm{d}\omega} = \frac{\mathrm{d}x + i\mathrm{d}y}{\mathrm{d}y} = \frac{\mathrm{d}x}{\mathrm{d}y} + i \tag{2.18}$$

where $u = \dfrac{\mathrm{d}x}{\mathrm{d}y}$ and $v = 1$. Since $\mathrm{d}x < 0$ and $\mathrm{d}y > 0$ then $u < 0$.

On CA, $\psi = q \wedge x = 0 \implies z = iy \wedge \omega = \varphi + iq$. Thus,

$$W = \frac{\mathrm{d}z}{\mathrm{d}\omega} = i\frac{\mathrm{d}y}{\mathrm{d}\varphi} \tag{2.19}$$

where $u = 0$ and $v = \dfrac{\mathrm{d}y}{\mathrm{d}\varphi}$.Since $\mathrm{d}y > 0$ and $\mathrm{d}\varphi < 0$ then $v < 0$. In addition, from CA to AB v

switches sign implying that A maps to 0.The above results in the domain shown in Fig 2.4.
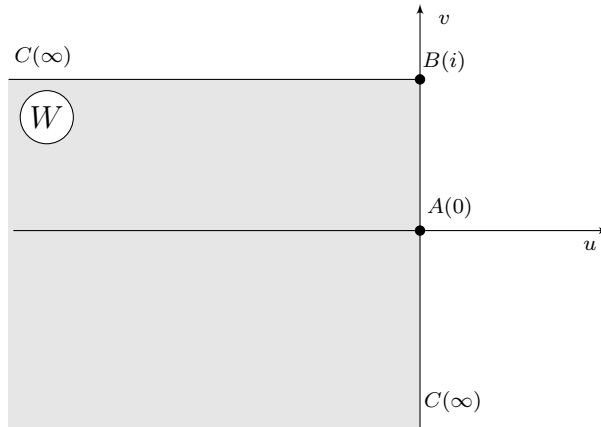
Figure 2.4: Domain in W-plane

Now, we map the domain in Figure 2.4 to the first quadrant.

$$W_1 = -W + i \tag{2.20}$$

From the mapping we get $B \mapsto 0, \quad C \mapsto \infty, \quad A \mapsto i.$
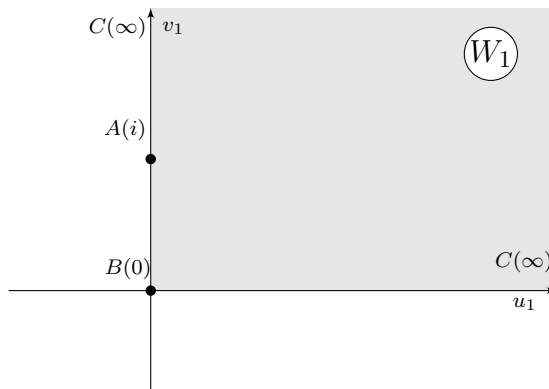
Figure 2.5: Domain in W_1- plane (First Quadrant)

We now consider the $\omega-$plane. We first rotate and scale the domain to something more usable

resulting in Figure 2.6.

$$\omega_1 = i\frac{\pi}{2q}\omega \tag{2.21}$$
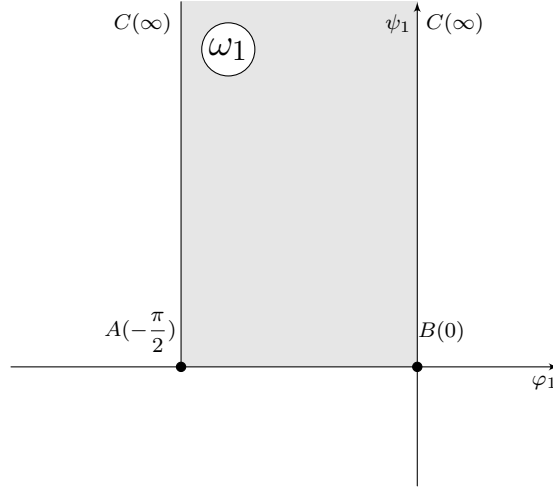
Figure 2.6: Domain in ω_1 - plane

From this domain we can then take the sine and rotate to get the first quadrant once more as seen

in Figure 2.7.

$$\omega_2 = -i\sin\left(i\frac{\pi}{2q}\omega\right) = \sinh\left(\frac{\pi}{2q}\omega\right) \tag{2.22}$$
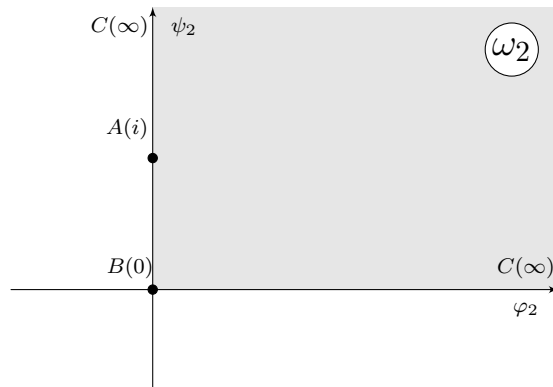
Figure 2.7: Domain in ω_2- plane (First Quadrant)

17

Now note that the ω_2 plane and W_1 planes just happen to be exactly the same, and by equating the two the following equation results.

$$-W + i = \sinh\left(\frac{\pi}{2q}\omega\right) \iff W = i - \sinh\left(\frac{\pi}{2q}\omega\right) \tag{2.23}$$

recall that $W = \dfrac{dz}{d\omega}$ which gives us the following

$$\frac{dz}{d\omega} = i - \sinh\left(\frac{\pi}{2q}\omega\right) \tag{2.24}$$

After some algebraic manipulation and integrating we get

$$z = i\omega - \frac{2q}{\pi}\cosh\left(\frac{\pi}{2q}\omega\right) + C. \tag{2.25}$$

To solve for C, we use the correspondence between point A and its image in the complex potential plane. Plugging into Eq.(2.25) results in

$$(0) = i(iq) - \frac{2q}{\pi}\cosh\left(\frac{\pi}{2q}(iq)\right) + C \tag{2.26}$$

From there, we conclude that $C = q$. The conformal mapping now has the following form

$$z = i\omega - \frac{2q}{\pi}\cosh\left(\frac{\pi}{2q}\omega\right) + q. \tag{2.27}$$

To find the relation between q and b we just have to plug in the point B on both sides which gets us

$$(b) = i(0) - \frac{2q}{\pi}\cosh\left(\frac{\pi}{2q}(0)\right) + q \tag{2.28}$$

18

Which results in the following equation that determines the exit point or length of the seepage surface.

$$b = q \left(1 - \frac{2}{\pi} \right) \tag{2.29}$$

From here, we can also plug in $z = x + iy$, and $\omega = \varphi + i\psi$ which results in the following

$$x + iy = i(\varphi + i\psi) - \frac{2q}{\pi} \cosh \left(\frac{\pi}{2q} (\varphi + i\psi) \right) + q. \tag{2.30}$$

From here we would like to solve for φ and ψ explicitly, but since that is not possible, we settle for x and y in terms of φ and ψ

$$x(\varphi, \psi) = q - \psi - \frac{2q}{\pi} \cosh \left(\frac{\pi}{2q} \varphi \right) \cos \left(\frac{\pi}{2q} \psi \right) \tag{2.31}$$

$$y(\varphi, \psi) = \varphi - \frac{2q}{\pi} \sinh \left(\frac{\pi}{2q} \varphi \right) \sin \left(\frac{\pi}{2q} \psi \right) \tag{2.32}$$

Now we can begin to investigate the boundary.

On BC, $\omega(z) = \varphi = y, \quad z = x + iy,$ and $y = h(x)$. Plugging this information in results in

$$x + ih(x) = ih(x) - \frac{2q}{\pi} \cosh \left(\frac{\pi}{2q} h(x) \right) + q. \tag{2.33}$$

After some simplification, we get the following shape and location for the phreatic surface.

$$h(x) = \frac{2q}{\pi} \text{arccosh} \left(\frac{-\pi}{2q} (x - q) \right) \tag{2.34}$$

On CA, $\omega(z) = \varphi + iq$, $z = iy$ which results in

$$y = \varphi - \frac{2q}{\pi} \sinh\left(\frac{\pi}{2q}\varphi\right). \tag{2.35}$$

Lastly on AB, $\omega(z) = i\psi$, $z = x$ which results in

$$x = q - \psi - \frac{2q}{\pi} \cos\left(\frac{\pi}{2q}\psi\right). \tag{2.36}$$
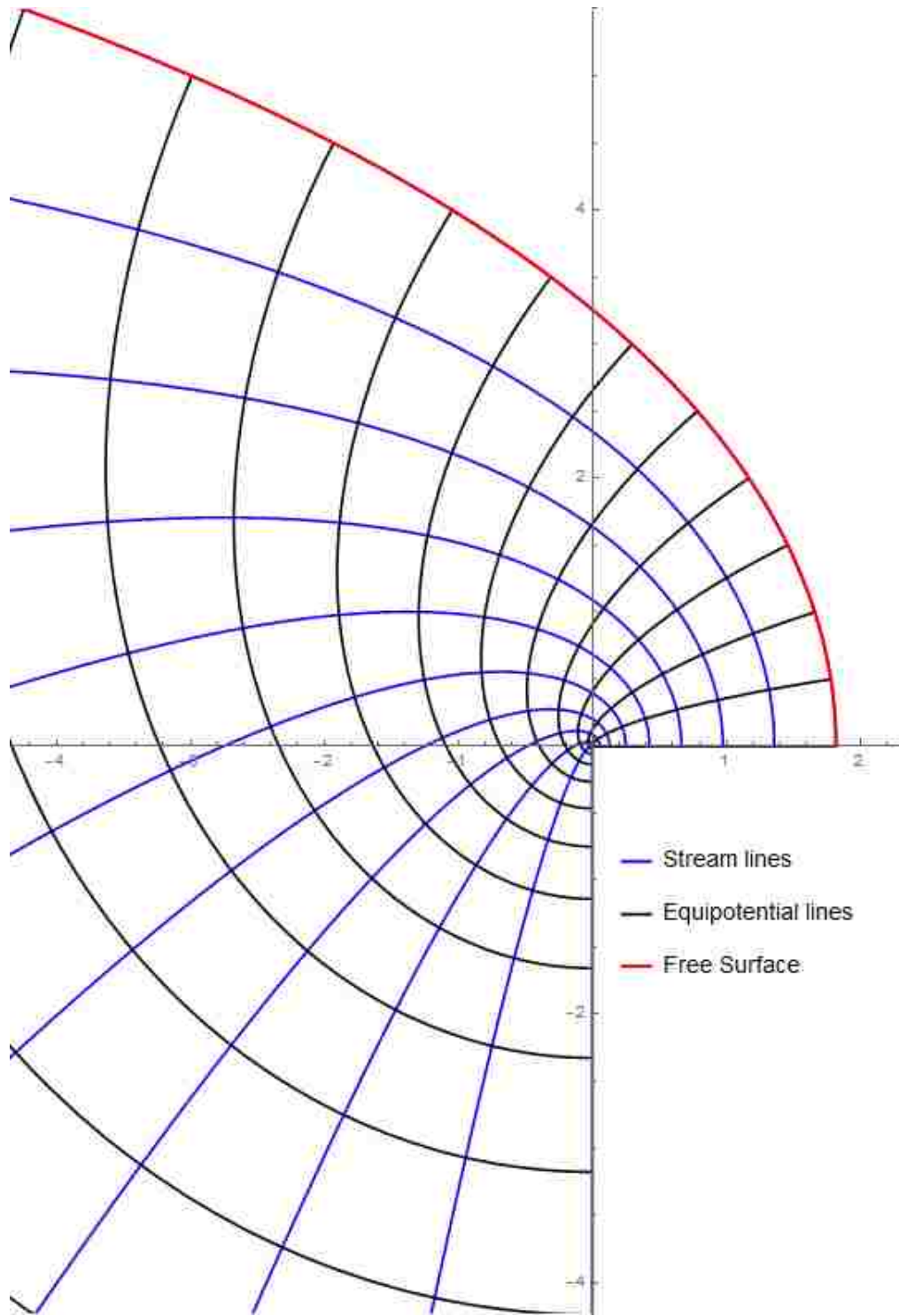
Figure 2.8: Flownet of Simplified Domain

2.5 The Phreatic Surface and Initial Guess for the Problem

We can see that Figure 2.1 should have approximately the same phreatic surface shape and location. The initial guess for the shape and location of the phreatic surface in both domains will come from the analytical solution. We use Eqs.(2.29) and (2.34) to derive what will become the initial guess of the phreatic surface. From Eq.(2.29), we solve for q in terms of b, the x-coordinate of the exit point, resulting in the following

$$q = \frac{\pi b}{\pi - 2}. \tag{2.37}$$

Solving Eq.(2.34) for x in terms of y results in

$$x = -\frac{2q}{\pi} \cosh\left(\frac{\pi}{2q} y\right) + q \tag{2.38}$$

plugging in the information from point C ($x = -\ell_1$ and $y = \ell_3$) into Eq.(2.38) results in

$$-\ell_1 = -\frac{2q}{\pi} \cosh\left(\frac{\pi}{2q}\ell_3\right) + q \tag{2.39}$$

Eq.(2.39) is then solved numerically for q. Let $q_0 > 0$ be the solution of Eq.(2.39) we then plug q_0 into Eq.(2.37) resulting in

$$q_0 = \frac{\pi b}{\pi - 2} \implies b = \frac{(\pi - 2)q_0}{2} \tag{2.40}$$

where b is used as the initial guess of the exit point for the iteration.

The rest of the initial guess for the phreatic surface is given by the piecewise function $g(x)$. Let

22

$\mu = -\ell_1 + \ell_3.$

$$g(x) = \begin{cases} -a(x + \ell_1)^2 + \ell_3, & -\ell_1 \leq x \leq \mu \\ \\ \alpha \operatorname{arccosh}(b + 1 - x), & \mu < x \leq b \end{cases} \tag{2.41}$$

where

$$a = \left(2\sqrt{b - \mu}\sqrt{2 + b - \mu} \operatorname{arccosh}(b + 1 - \mu) + \ell_3 \right)^{-1} \tag{2.42}$$

and

$$\alpha = \frac{2\ell_3\sqrt{b - \mu}\sqrt{2 + b - \mu}}{2\sqrt{b - \mu}\sqrt{2 + b - \mu} \operatorname{arccosh}(b + 1 - \mu) + \ell_3} \tag{2.43}$$

are chosen to guarantee continuity and differentiability at the transition point. The upper part of Eq.(2.41) is chosen to keep point C a regular point which requires that line BC and line CD intersect at an angle of $\dfrac{\pi}{2}$. The lower part of Eq.(2.41) is chosen for a similar reason with line AB and curve BC, but also because the analytic solution from the conformal mapping was an inverse hyperbolic function.

2.6   Algorithm for Determination of the Location of the Phreatic Surface

In Liggett and Liu (1983), an efficient algorithm was proposed for locating a phreatic surface in a domain modeling a dam with tail water (vertical exit). Chantasiriwan (2011) applied this algorithm inside of another iterative process for locating a phreatic surface in a domain modeling a dam with toe drain (horizontal exit). The main idea of Chantasiriwan's 2011 paper is that instead of directly solving a seepage problem in Figure 2.9, they solve the seepage problem in Figure 2.10. It is important to note that $\Delta x' < \Delta x$, so that a new vertical boundary Γ_3 is formed.

This algorithm will be implemented with our seepage problem resulting in Figure 2.11 with $b' < b$. b'' is determined initially as $g(b')$ from Eq.(2.41). B' is then fixed and the BVP is solved as
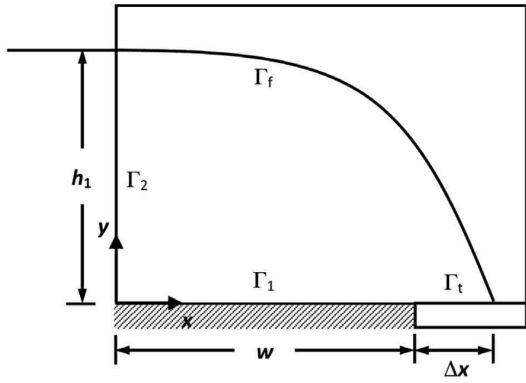
Figure 2.9: Model of Dam with Toe Drain (Chantasiriwan, 2011)
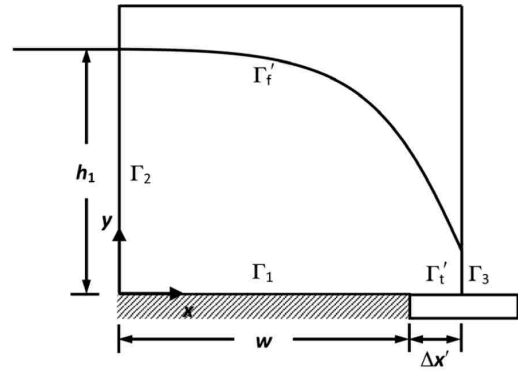
Figure 2.10: Model of Dam with Seepage Surface and Toe Drain (Chantasiriwan, 2011)

a traditional tail water problem. The iteration used here is $y_{j+1} = \dfrac{y_j + u_j}{2}$ where u_j is the value of ϕ given from the jth iteration of the BEM. Bruch (1991) states that this weighted iteration has been shown to be more stable for underground water flow. After this iteration is done, the other iteration adjusts the location of b'. Chantasiriwan (2011) states that this algorithm would then ideally result with $\Gamma_3 = 0$ thus solving the the original seepage problem. However, he notes that practically there is a non-zero minimum value for which the iteration becomes unstable.

24
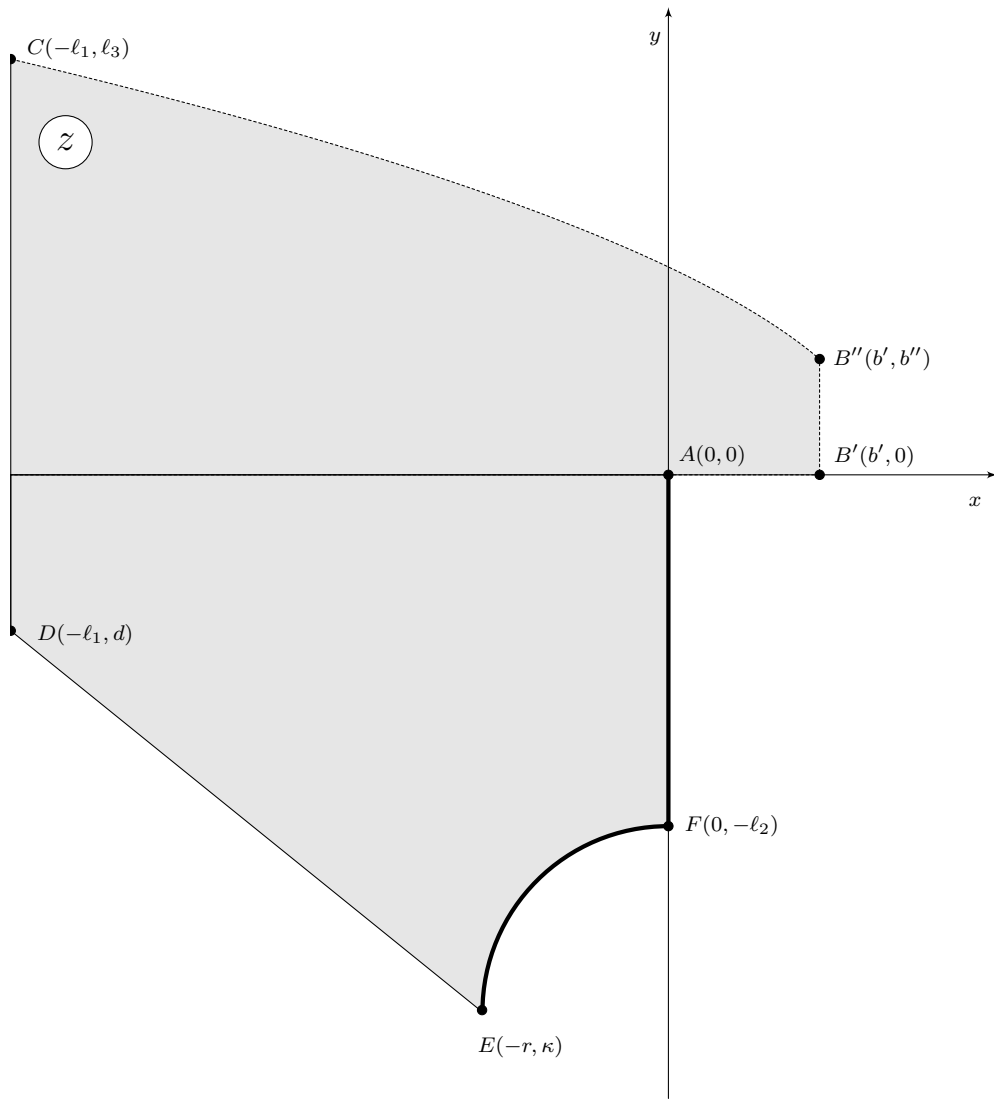
Figure 2.11: Modified Physical Domain, z-plane.

CHAPTER 3

THE TRADITIONAL BOUNDARY ELEMENT METHOD

In order to use the BEM as outlined in Section 2.2 to find the solution $\phi(x, y)$ of the BVP in Section 2.1, we need to discretize the domain in Figure 2.1. The discretization of the domain is done as follows: AB$'$ is discretized into k_1 elements, B$'$B$''$ is discretized into k_7 elements, B$''$C is discretized into k_2 elements then the first element is further subdivided into k_8 elements, CD is discretized into k_3 elements, DE is discretized into k_4 elements, EF is discretized into k_5 elements, and FA is discretized into k_6 elements. Due to the kind of singularity at points A, D, and E, instead of having one node at each point, there are two nodes that approach each point using discontinuous elements adjacent to the points. The total number of nodes is $N = k_1 + k_2 + k_7 + k_8 - 1 + k_3 + 1 + k_4 + 1 + k_5 + k_6 + 1$. For clarity purposes the following notation will also be introduced: $K_1 = k_1$, $K_7 = k_1 + k_7$, $K_2 = K_7 + k_8 - 1 + k_2$, $K_3 = k_3 + K_2$, $K_4 = k_4 + 1 + K_3$, $K_5 = k_5 + 1 + K_4$, $K_6 = k_6 + 1 + K_5$. The integrals from Eq.(2.7) for each part of the boundary are now developed. All indexed integrals are defined and solved in the Appendix.

3.1 Assembly of Integrals on Line Segment AB$'$

On AB$'$, $\phi(x, 0) = 0$, $\varepsilon_1 < x < b'$ thus

$$\frac{\partial \phi}{\partial n} = \Omega = \Omega_m \left(\frac{x_{m+1} - x}{x_{m+1} - x_m} \right) + \Omega_{m+1} \left(\frac{x - x_m}{x_{m+1} - x_m} \right)$$

and $r_p = \sqrt{(x - x_p)^2 + y_p^2}$. From Eq.(2.7), one gets

$$I_{m,m+1}^{(p)} = -\Omega_m \int_{x_m}^{x_{m+1}} \left(\frac{x_{m+1} - x}{x_{m+1} - x_m} \right) \ln \sqrt{(x - x_p)^2 + y_p^2} \, dx$$

$$- \Omega_{m+1} \int_{x_m}^{x_{m+1}} \left(\frac{x - x_m}{x_{m+1} - x_m} \right) \ln \sqrt{(x - x_p)^2 + y_p^2} \, dx. \tag{3.1}$$

After integration, Eq.(3.1) becomes

$$I_{m,m+1}^{(p)} = -\Omega_m I_1(x_m, x_{m+1}, x_p, |y_p|) + \Omega_{m+1} I_1(x_{m+1}, x_m, x_p, |y_p|). \tag{3.2}$$

Then, by using Eqs.(2.15) and (2.16), we get

$$a_{p,m}^{(m)} = -I_1(x_m, x_{m+1}, x_p, |y_p|) \tag{3.3}$$

$$a_{p,m}^{(m-1)} = I_1(x_m, x_{m-1}, x_p, |y_p|). \tag{3.4}$$

3.2   Assembly of Integrals on Line Segment B′B″

On B′B″, $\phi(b', y) = y,$ $0 < y < b''$ thus

$$\frac{\partial \phi}{\partial n} = \Omega = \Omega_m \left(\frac{y_{m+1} - y}{y_{m+1} - y_m} \right) + \Omega_{m+1} \left(\frac{y - y_m}{y_{m+1} - y_m} \right),$$

$$r_p = \sqrt{(b' - x_p)^2 + (y - y_p)^2},$$

and $\dfrac{\partial r_p}{\partial n}(b', y) = \dfrac{b' + x_p}{\sqrt{(b' + x_p)^2 + (y - y_p)^2}}.$ From Eq.(2.7), one gets

$$I_{m,m+1}^{(p)} = \int_{y_m}^{y_{m+1}} \frac{(b' + x_p)y}{(b' + x_p)^2 + (y - y_p)^2} \, dy$$

$$- \Omega_m \int_{y_m}^{y_{m+1}} \left(\frac{y_{m+1} - y}{y_{m+1} - y_m} \right) \ln \sqrt{(b' - x_p)^2 + (y - y_p)^2} \, dy$$

$$- \Omega_{m+1} \int_{y_m}^{y_{m+1}} \left(\frac{y - y_m}{y_{m+1} - y_m} \right) \ln \sqrt{(b' - x_p)^2 + (y - y_p)^2} \, dy. \tag{3.5}$$

27

After integration, Eq.(3.5) becomes

$$I^{(p)}_{m,m+1} = -\Omega_m\, I_1(y_m, y_{m+1}, y_p, |b' - x_p|) + \Omega_{m+1}\, I_1(y_{m+1}, y_m, y_p, |b' - x_p|). \tag{3.6}$$

Then, by using Eq.(2.15) and (2.16), we get

$$a^{(m)}_{p,m} = -I_1(y_m, y_{m+1}, y_p, |b' - x_p|) \tag{3.7}$$

$$a^{(m-1)}_{p,m} = I_1(y_m, y_{m-1}, y_p, |b' - x_p|) \tag{3.8}$$

$$B_{p,m} = -b''\, I_2(b'', 0, y_p, b' + x_p). \tag{3.9}$$

3.3 Assembly of Integrals on Phreatic Surface B''C

On B''C , $\phi(x, g(x)) = g(x) \,\wedge\, \dfrac{\partial \phi}{\partial n}(x, g(x)) = 0, \quad -\ell_1 < x < b'$ thus

$$\phi = \Omega = \Omega_m \left(\frac{x_{m+1} - x}{x_{m+1} - x_m} \right) + \Omega_{m+1} \left(\frac{x - x_m}{x_{m+1} - x_m} \right).$$

The following substitutions are made:

$c_m = x_m - x_{m+1}$

$d_m = y_{m+1} - y_m$

$g_m = \sqrt{c_m^2 + d_m^2}$

$f_{p,m} = \dfrac{d_m(x_p - x_m) + c_m(y_p - y_m)}{g_m}$

$F_{p,m} = \dfrac{f_{p,m}}{g_m}.$

From Eq.(2.7), we get

$$I^{(p)}_{m,m+1} = -\frac{g_m}{c_m} \int_{x_m}^{x_{m+1}} \frac{\phi}{r_p} \frac{\partial r_p}{\partial n}\, dx. \tag{3.10}$$

28

It should be noted that the free-surface is approximated as a series of connected line segments with

the equations

$$y = y_m - \frac{d_m}{c_m}(x - x_m).$$ (3.11)

From here we may consider

$$\frac{\partial r_p}{\partial n} = \frac{\partial r_p}{\partial x}\frac{d_m}{g_m} + \frac{\partial r_p}{\partial y}\frac{c_m}{g_m} = \frac{d_m(x - x_p) + c_m(y - y_p)}{g_m r_p}$$ (3.12)

plugging in results in Eq.(3.10) becoming

$$I_{m,m+1}^{(p)} = -\frac{1}{c_m}\int_{x_m}^{x_{m+1}}\phi\frac{d_m(x - x_p) + c_m(y - y_p)}{r_p^2}\,dx.$$ (3.13)

the choice of substitutions and Eq.(3.11) yields a convenient expression for r_p^2

$$r_p^2 = (x - x_p)^2 - (y - y_p)^2 = (x - x_p)^2 - \left(\frac{d_m}{c_m}(x - x_m) + y_p - y_m\right)^2$$

$$= \frac{g_m^2}{c_m^2}\left((x - x_p + d_m F_{p,m})^2 + (c_m F_{p,m})^2\right)$$ (3.14)

we also have another convenient relation

$$-g_m f_{m,p} = d_m(x_m - x_p) + c_m(y_m - y_p) = d_m(x - x_p) + c_m(y - y_p)$$ (3.15)

plugging Eqs.(3.14) and (3.15) into Eq.(3.13) results in

$$I_{m,m+1}^{(p)} = c_m F_{p,m}\int_{x_m}^{x_{m+1}}\frac{\phi}{(x - x_p + d_m F_{p,m})^2 + (c_m F_{p,m})^2}\,dx$$ (3.16)

(Muleshkov, 1988). From here, we note

$$I_{m,m+1}^{(p)} = \frac{c_m F_{p,m}}{c_m} \int_{x_m}^{x_{m+1}} \frac{-\Omega_m(x_{m+1} - x) - \Omega_{m+1}(x - x_m)}{(x - x_p + d_m F_{p,m})^2 + (c_m F_{p,m})^2} \, dx. \tag{3.17}$$

Therefore,

$$I_{m,m+1}^{(p)} = \Omega_m I_2(x_m, x_m + 1, x_p - d_m F_{p,m}, |c_m F_{p,m}|) - \Omega_{m+1} I_2(x_{m+1}, x_m, x_p - d_m F_{p,m}, |c_m F_{p,m}|) \tag{3.18}$$

Then, by using Eqs.(2.15) and (2.16), we get

$$a_{p,m}^{(m)} = I_2(x_m, x_{m+1}, x_p - d_m F_{p,m}, |c_m F_{p,m}|) \tag{3.19}$$

$$a_{p,m}^{(m-1)} = -I_2(x_m, x_{m-1}, x_p - d_{m-1} F_{p,m-1}, |c_{m-1} F_{p,m-1}|). \tag{3.20}$$

3.4   Assembly of Integrals on Line Segment CD

On CD, $\phi(-\ell_1, y) = \ell_3$, $\quad d + \varepsilon_3 < y < \ell_3$ thus

$$\frac{\partial \phi}{\partial n} = \Omega = \Omega_m \left(\frac{y_{m+1} - y}{y_{m+1} - y_m} \right) + \Omega_{m+1} \left(\frac{y - y_m}{y_{m+1} - y_m} \right),$$

$$r_p = \sqrt{(-\ell_1 - x_p)^2 + (y - y_p)^2},$$

and $\dfrac{\partial r_p}{\partial n}(-\ell_1, y) = \dfrac{\ell_1 + x_p}{\sqrt{(\ell_1 + x_p)^2 + (y - y_p)^2}}$. From Eq.(2.7), one gets

$$I_{m,m+1}^{(p)} = -\ell_3 \int_{y_m}^{y_{m+1}} \frac{\ell_1 + x_p}{(\ell_1 + x_p)^2 + (y - y_p)^2} \, dy$$

$$+ \Omega_m \int_{y_m}^{y_{m+1}} \left(\frac{y_{m+1} - y}{y_{m+1} - y_m} \right) \ln \sqrt{(\ell_1 + x_p)^2 + (y - y_p)^2} \, dy$$

$$+ \Omega_{m+1} \int_{y_m}^{y_{m+1}} \left(\frac{y - y_m}{y_{m+1} - y_m} \right) \ln \sqrt{(\ell_1 + x_p)^2 + (y - y_p)^2} \, dy. \tag{3.21}$$

30

After integration, Eq.(3.21) becomes

$$I_{m,m+1}^{(p)} = -I_3(y_m, y_{m+1}, y_p, \ell_1 + x_p) + \Omega_m I_1(y_m, y_{m+1}, y_p, \ell_1 + x_p) + \Omega_{m+1} I_1(y_{m+1}, y_m, y_p, \ell_1 + x_p).$$

(3.22)

Then, by using Eqs.(2.15), (2.16) and (2.9), we get

$$a_{p,m}^{(m)} = I_1(y_m, y_{m+1}, y_p, \ell_1 + x_p) \tag{3.23}$$

$$a_{p,m}^{(m-1)} = -I_1(y_m, y_{m-1}, y_p, \ell_1 + x_p) \tag{3.24}$$

$$B_{p,m} = -I_3(y_m, y_{m+1}, y_p, \ell_1 + x_p). \tag{3.25}$$

3.5 Assembly of Integrals on Line Segment DE

On DE, $\phi(x, -x - \ell_2 - 2r) = \ell_3, \quad -\ell_1 + \varepsilon_4 < x < -r$

$$\frac{\partial \phi}{\partial n} = \Omega = \Omega_m \left(\frac{x_{m+1} - x}{x_{m+1} - x_m} \right) + \Omega_{m+1} \left(\frac{x - x_m}{x_{m+1} - x_m} \right).$$

The substitution $s_p = \ell_2 + 2r + y_p + x_p$ is made, thus

$$r_p = \sqrt{(x - x_p)^2 + (y - y_p)^2} = \sqrt{(x - x_p)^2 + (x + \ell_2 + 2r + y_p)^2}$$

$$= \sqrt{2} \sqrt{\left(x - x_p + \frac{1}{2} s_p \right)^2 + \left(\frac{s_p}{2} \right)^2}. \tag{3.26}$$

On DE, we also have

$$\frac{\partial r_p}{\partial n} = \left\langle \frac{-1}{\sqrt{2}}, \frac{-1}{\sqrt{2}} \right\rangle \cdot \left\langle \frac{\partial r_p}{\partial x}, \frac{\partial r_p}{\partial y} \right\rangle = \frac{-1}{\sqrt{2}} \left(\frac{x - x_p}{r_p} + \frac{y - y_p}{r_p} \right) = \frac{s_p}{\sqrt{2} r_p}. \tag{3.27}$$

31

From Eq.(2.7), one gets

$$
\begin{aligned}
I^{(p)}_{m,m+1} = {} & \frac{\ell_3}{2} \int_{x_m}^{x_{m+1}} \frac{s_p}{\left(x - x_p + \frac{1}{2}s_p\right)^2 + \left(\frac{s_p}{2}\right)^2} \, dx \\
& - \sqrt{2}\Omega_m \int_{x_m}^{x_{m+1}} \left(\frac{x_{m+1} - x}{x_{m+1} - x_m}\right) \ln\left(\sqrt{2}\sqrt{\left(x - x_p + \frac{1}{2}s_p\right)^2 + \left(\frac{s_p}{2}\right)^2}\right) dx \\
& + \sqrt{2}\Omega_{m+1} \int_{x_m}^{x_{m+1}} \left(\frac{x - x_m}{x_{m+1} - x_m}\right) \ln\left(\sqrt{2}\sqrt{\left(x - x_p + \frac{1}{2}s_p\right)^2 + \left(\frac{s_p}{2}\right)^2}\right) dx.
\end{aligned}
\tag{3.28}
$$

From here, it can be shown that

$$
a^{(m)}_{p,m} = -\frac{\ln 2}{\sqrt{8}}(x_{m+1} - x_m) - \sqrt{2}I_1\left(x_m, x_{m+1}, x_p - \frac{1}{2}s_p, \frac{s_p}{2}\right)
\tag{3.29}
$$

$$
a^{(m-1)}_{p,m} = \frac{\ln 2}{\sqrt{8}}(x_{m-1} - x_m) + \sqrt{2}I_1\left(x_m, x_{m-1}, x_p - \frac{1}{2}s_p, \frac{s_p}{2}\right)
\tag{3.30}
$$

$$
B_{p,m} = \ell_3 I_3\left(x_m, x_{m+}, x_p - \frac{1}{2}s_p, \frac{s_p}{2}\right).
\tag{3.31}
$$

3.6   Assembly of Integrals on Arc EF

On EF, $\dfrac{\partial \phi}{\partial n}(R\cos\theta, R\sin\theta + \kappa) = 0$, $\kappa = -\ell_2 - R$, $\dfrac{\pi}{2} < \theta < \pi$.

Thus $\phi = \Omega = \Omega_m \left(\dfrac{\theta_{m+1} - \theta}{\theta_{m+1} - \theta_m}\right) + \Omega_{m+1}\left(\dfrac{\theta - \theta_m}{\theta_{m+1} - \theta_m}\right)$.

Since $x = R\cos\theta$ and $y = R\sin\theta + \kappa$, we have

$$
r_p = \sqrt{(R\cos\theta - x_p)^2 + (R\sin\theta - (y_p - \kappa))^2}
\tag{3.32}
$$

and

$$
\frac{\partial r_p}{\partial n} = -\frac{1}{r_p}\left((R\cos\theta - x_p)\cos\theta + (R\sin\theta - (y_p - \kappa))\sin\theta\right)
\tag{3.33}
$$

From Eq.(2.7), one gets

$$I_{m,m+1}^{(p)} = \Omega_m \int_{\theta_m}^{\theta_{m+1}} \left(\frac{\theta_{m+1} - \theta}{\theta_{m+1} - \theta_m} \right) \frac{(R\cos\theta - x_p)\cos\theta + (R\sin\theta - (y_p - \kappa))\sin\theta}{(R\cos\theta - x_p)^2 + (R\sin\theta - (y_p - \kappa))^2} r d\theta$$

$$+ \Omega_{m+1} \int_{\theta_m}^{\theta_{m+1}} \left(\frac{\theta - \theta_m}{\theta_{m+1} - \theta_m} \right) \frac{(R\cos\theta - x_p)\cos\theta + (R\sin\theta - (y_p - \kappa))\sin\theta}{(R\cos\theta - x_p)^2 + (R\sin\theta - (y_p - \kappa))^2} r d\theta$$

(3.34)

$$= \Omega_m \int_{\theta_m}^{\theta_{m+1}} \left(\frac{\theta_{m+1} - \theta}{\theta_{m+1} - \theta_m} \right) \frac{R^2 - x_p R\cos\theta - (y_p - \kappa)R\sin\theta}{(R\cos\theta - x_p)^2 + (R\sin\theta - (y_p - k))^2} d\theta$$

$$+ \Omega_{m+1} \int_{\theta_m}^{\theta_{m+1}} \left(\frac{\theta_{m+1} - \theta}{\theta_{m+1} - \theta_m} \right) \frac{R^2 - x_p R\cos\theta - (y_p - \kappa)R\sin\theta}{(R\cos\theta - x_p)^2 + (R\sin\theta - (y_p - \kappa))^2} d\theta.$$

(3.35)

From here, it can be shown that

$$a_{p,m}^{(m)} = I_7(\theta_m, \theta_{m+1}, x_p, y_p - \kappa, R)$$

(3.36)

$$a_{p,m}^{(m-1)} = -I_7(\theta_m, \theta_{m-1}, x_p, y_p - \kappa, R).$$

(3.37)

3.7 Assembly of Integrals on Line Segment FA

On FA, $\frac{\partial \phi}{\partial n}(0, y) = 0 \quad -\ell_2 < y < \varepsilon_2$.

Thus $\phi = \Omega = \Omega_m \left(\frac{y_{m+1} - y}{y_{m+1} - y_m} \right) + \Omega_{m+1} \left(\frac{y - y_m}{y_{m+1} - y_m} \right)$,

$r_p(0, y) = \sqrt{(-x_p)^2 + (y - y_p)^2}$,

and $\frac{\partial r_p}{\partial n}(0, y) = \frac{-x_p}{\sqrt{(-x_p)^2 + (y - y_p)^2}}$. From Eq.(2.7), one gets

$$I_{m,m+1}^{(p)} = -\Omega_m \int_{y_m}^{y_{m+1}} \left(\frac{y_{m+1} - y}{y_{m+1} - y_m} \right) \frac{x_p}{x_p^2 + (y - y_p)^2} dy$$

$$- \Omega_{m+1} \int_{y_m}^{y_{m+1}} \left(\frac{y - y_m}{y_{m+1} - y_m} \right) \frac{x_p}{x_p^2 + (y - y_p)^2} dy$$

(3.38)

33

After integration, Eq.(3.38) becomes

$$I^{(p)}_{m,m+1} = -\Omega_m\, I_2(y_m, y_{m+1}, y_p, |x_p|) + \Omega_{m+1}\, I_2(y_{m+1}, y_m, y_p, |x_p|). \tag{3.39}$$

Then, by using Eqs.(2.15) and (2.16), we get

$$a^{(m)}_{p,m} = -I_2(y_m, y_{m+1}, y_p, |x_p|) \tag{3.40}$$

$$a^{(m-1)}_{p,m} = I_2(y_m, y_{m-1}, y_p, |x_p|). \tag{3.41}$$

CHAPTER 4

THE MODIFIED BOUNDARY ELEMENT METHOD

4.1   Treatment of the Singularity at Point A

The local behavior around the singular point A is found. We consider the infinite extension of the adjacent sides of point A in the domain in Figure 2.1 preserving the boundary conditions, shown in Figure 4.1. The corresponding domain in the complex potential plane of the domain in Figure 4.1 is shown Figure 4.2.

Figure 4.1:   Extension of Boundary Near Point A
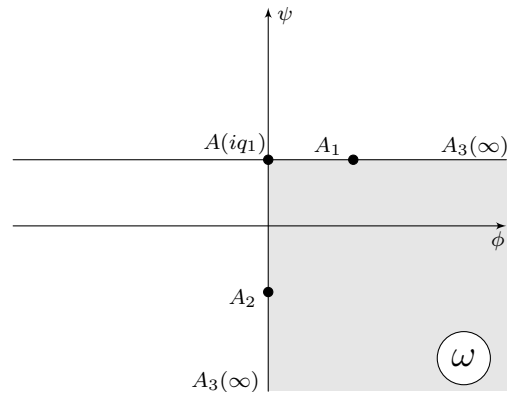
Figure 4.2:   Domain in Complex Potential Plane of Figure 4.1

The conformal mapping that maps the domain in Figure 4.1 to the corresponding domain in Figure 4.2 is

$$\omega = -iM_1 \sqrt[3]{z} + iq_1 \tag{4.1}$$

where M_1 and q_1 are arbitrary real numbers. Using Eq.(4.1) and any choice of M_1 and q_1 results in the the flow net in Figure 4.3. Since $\omega = \phi + i\psi$, $\phi(x,y)$ is the real part of ω. Thus, if $z = re^{i\theta}$, we get

$$\phi(x,y) = M_1 \sqrt[3]{r} \cos\left(\frac{\theta}{3} + \frac{3\pi}{2}\right) \tag{4.2}$$

as the solution of the BVP for the domain shown in Figure 4.1.
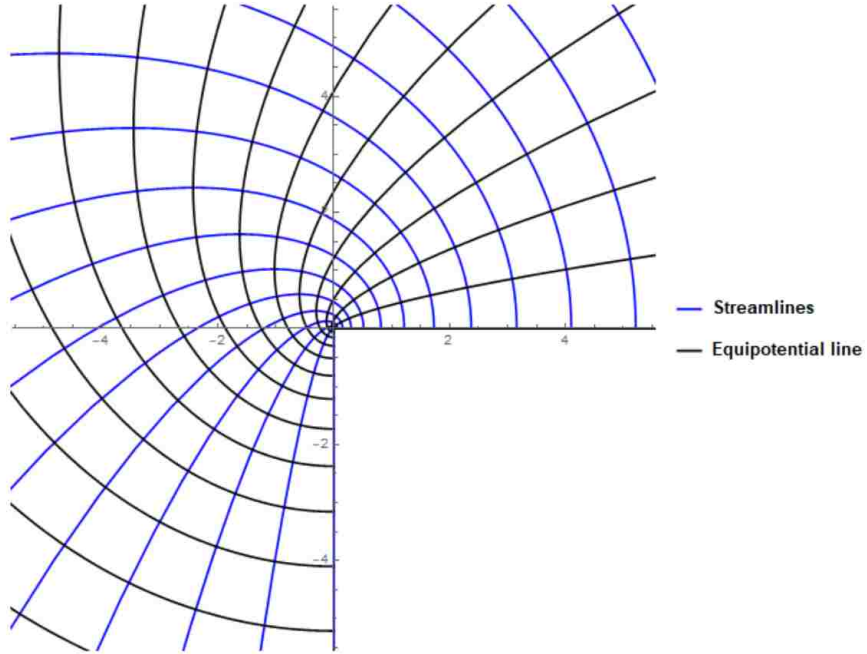
Figure 4.3: Flownet of Domain in Figure 4.1

On Segment A_1A (from node $K_6 - 2$ to $K_6 - 1$), $\theta = \dfrac{3\pi}{2}$ and $r = -y$, hence

$$\Omega = \phi = M_1 \sqrt[3]{-y} \tag{4.3}$$

At A_1, $y = y_{K_6-2}$, so

$$\Omega_{K_6-2} = M_1 \sqrt[3]{-y_{K_6-2}} \implies M_1 = \frac{\Omega_{K_6-2}}{\sqrt[3]{-y_{K_6-2}}} \tag{4.4}$$

Therefore,

$$\Omega = \phi = \frac{\Omega_{K_6-2}}{\sqrt[3]{-y_{K_6-2}}} \sqrt[3]{-y} \tag{4.5}$$

Using Eq.(4.5), Eq.(2.7) becomes

$$I_{K_6-2,K_6-1}^{(p)} = -\frac{\Omega_{K_6-2}x_p}{\sqrt[3]{-y_{K_6-2}}} \int_{y_{K_6-2}}^{y_{K_6-1}} \frac{\sqrt[3]{-y}}{(y-y_p)^2 + x_p^2} \, dy \tag{4.6}$$

$$= \frac{-3x_p\Omega_{K_6-2}}{\sqrt[3]{-y_{K_6-2}}} I_4(y_p, x_p, \sqrt[3]{-y_{K_6-2}}) \tag{4.7}$$

Thus, one gets

$$a_{p,K_6-2}^{(K_6-2)} = \frac{-3x_p}{\sqrt[3]{-y_{K_6-2}}} I_4(y_p, x_p, \sqrt[3]{-y_{K_6-2}}) \tag{4.8}$$

to be used as a replacement to what was found using the traditional method. Ω_{K_6-1} is excluded from the system in the modified BEM.

On Segment AA_2 (from node 0 to 1), $y = 0$, $\theta = \arctan\left(\frac{y}{x}\right) = 0$, $\frac{\partial r}{\partial y} = 0$, and $\frac{\partial \theta}{\partial y} = \frac{1}{x}$. Hence

$$\Omega = \frac{\partial \phi}{\partial n} = -\frac{\partial \phi}{\partial y} = -\frac{M_2}{3} \frac{1}{\sqrt{x^2}} \tag{4.9}$$

At A_2, $x = x_1$, so

$$\Omega_1 = -\frac{M_2}{3} \frac{1}{\sqrt{x_1^2}} \implies M_2 = -3\Omega_1 \sqrt[3]{x_1^2} \tag{4.10}$$

Therefore,

$$\Omega = \frac{\partial \phi}{\partial n} = \Omega_1 \sqrt[3]{\left(\frac{x_1}{x}\right)^2} \tag{4.11}$$

37

Using Eq.(4.11), Eq.(2.7) becomes

$$
\begin{aligned}
I_{0,1}^{(p)} &= \Omega_1 \int_{x_0}^{x_1} \sqrt[3]{\frac{x_1^2}{x^2}} \ln \sqrt{(x - x_p)^2 + y_p^2} \, dx \\
&= \frac{\Omega_1}{2} \sqrt[3]{x_1^2} \left(3 \sqrt[3]{x} \ln \left((x - x_p)^2 + y_p^2 \right) \right) \Big|_0^{x_1} - 3 \sqrt[3]{x_a^2} \Omega_1 \int_0^{x_1} \sqrt[3]{x} \frac{(x - x_p)}{(x - x_p)^2 + y_p^2} \, dx \\
&= \frac{3\Omega_1}{2} x_1 \sqrt[3]{x_1} \ln \left((x_1 - x_p)^2 + y_p^2 \right) - 9 \sqrt[3]{x_1^2} \Omega_1 \int_0^{\sqrt[3]{x_1}} \frac{u^6 - x_p u^3}{(u^3 - x_p)^2 + y_p^2} \, du \\
&= \frac{3\Omega_1}{2} x_1 \sqrt[3]{x_1} \ln \left((x_1 - x_p)^2 + y_p^2 \right) - 9 \sqrt[3]{x_1^2} \Omega_1 \left(\frac{\sqrt[3]{x_1^4}}{3y_p} I_5(x_p, y_p, \sqrt[3]{x_1}) - x_p I_4^*(x_p, y_p, \sqrt[3]{x_1}) \right) \\
&= \frac{3\Omega_1}{2} x_1 \sqrt[3]{x_1} \ln \left((x_1 - x_p)^2 + y_p^2 \right) - \frac{3x_1^2}{y_p} \Omega_1 I_5(x_p, y_p, \sqrt[3]{x_1}) - x_p \Omega_1 I_4(x_p, y_p, \sqrt[3]{x_1}) \qquad (4.12)
\end{aligned}
$$

Thus, one gets

$$
a_{p,1}^{(1)} = \frac{3}{2} x_1 \sqrt[3]{x_1} \ln \left((x_1 - x_p)^2 + y_p^2 \right) - \frac{3x_1^2}{y_p} I_5(x_p, y_p, \sqrt[3]{x_1}) - x_p I_4(x_p, y_p, \sqrt[3]{x_1}) \qquad (4.13)
$$

to be used as a replacement to what was found using the traditional method. Ω_0 is excluded from the system in the modified BEM.

4.2   Treatment of the Singularity at Point D

The local behavior near the singular point D is found. We consider the infinite extension of the sides of point D in Figure 2.1 preserving the boundary conditions, shown in Figure 4.4. The corresponding domain in the complex potential plane of the domain in Figure 4.4 is shown in Figure 4.5.
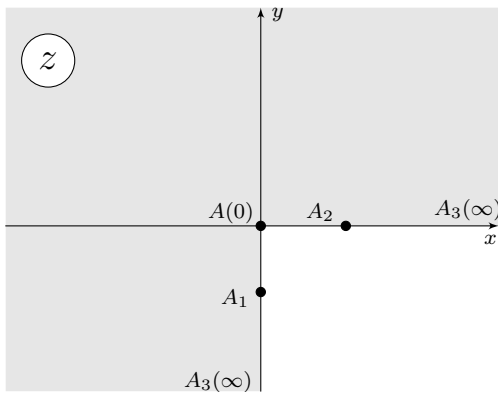
The conformal mapping that maps the domain in Figure 4.4 to the domain in Figure 4.5 is

$$
\omega = M_3 e^{\frac{5\pi}{6} i} (z + \ell_1 - di)^{4/3} + \ell_3 + q_2 i \qquad (4.14)
$$

38
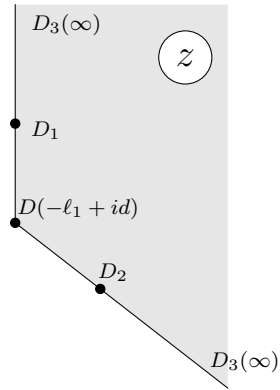
Figure 4.4: Extension of Boundary Near Point D
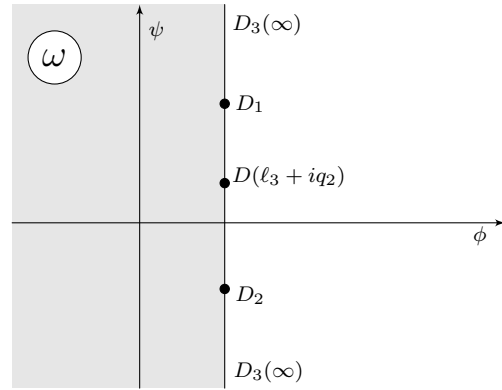
Figure 4.5: Domain in Complex Potential Plane of Figure 4.4

where M_3 and q_2 are arbitrary real numbers. Using Eq.(4.14) and any choice for M_3 and q_2 results in the flow net in Figure 4.6. Since $\omega = \phi + i\psi$, $\phi(x, y)$ is the real part of ω. Thus, if $z = re^{i\theta}$, we get

$$\phi(x, y) = M_3 r^{\frac{4}{3}} \cos\left(\frac{4\theta}{3} + \frac{5\pi}{6}\right) + \ell_3 \tag{4.15}$$

as the solution of the BVP for the domain shown in Figure 4.4.
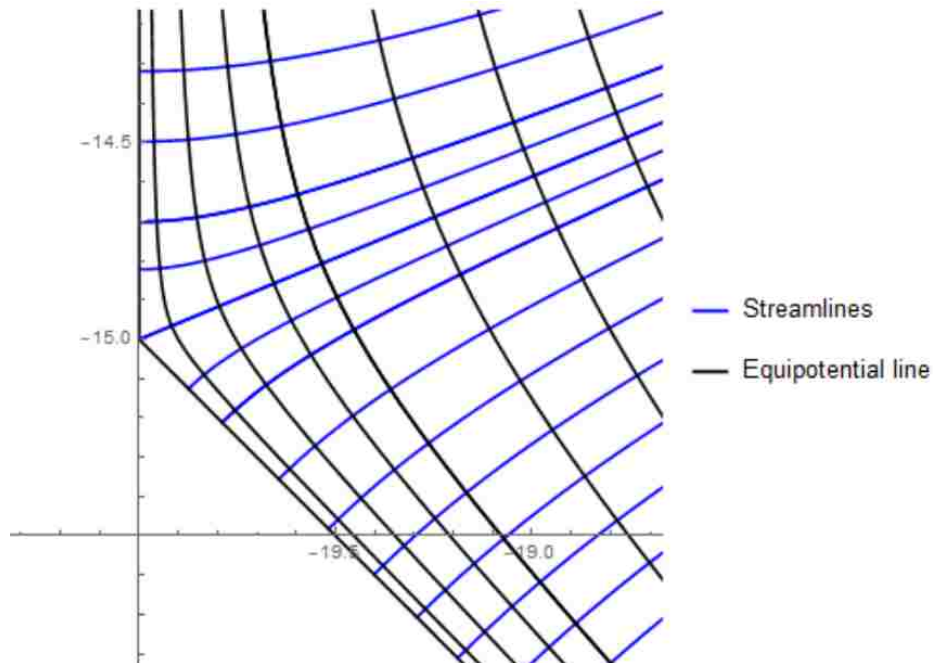
Figure 4.6: Flownet of Domain in Figure 4.4

On Segment D_1D (from node $K_3 - 1$ to K_3),

$x = -\ell_1,\ \theta = \dfrac{\pi}{2},\ r = y - d,\ \dfrac{\partial\theta}{\partial x} = \dfrac{1}{d - y}$, and $\dfrac{\partial r}{\partial x} = 0$. Hence,

$$\Omega = \frac{\partial\phi}{\partial n} = -\frac{\partial\phi}{\partial x} = \frac{4M_3}{3}\sqrt[3]{y - d} \tag{4.16}$$

At D_1, $y = y_{K_3-1}$, so

$$\Omega_{K_3-1} = \frac{4M_3}{3}\sqrt[3]{y_{K_3-1} - d} \implies M_3 = \frac{3\Omega_{K_3-1}}{4\sqrt[3]{y_{K_3-1} - d}} \tag{4.17}$$

Therefore,

$$\Omega = -\frac{\partial\phi}{\partial x} = \Omega_{K_3-1}\sqrt[3]{\frac{y - d}{y_{K_3-1} - d}} \tag{4.18}$$

Using Eq.(4.18), Eq.(2.7) becomes

$$I_{K_3-1,K_3}^{(p)} = B_{p,K_3-1} + \Omega_{K_3-1}\int_{y_{K_3-1}}^{y_{K_3}}\sqrt[3]{\frac{y - d}{y_{K_3-1} - d}}\ln\sqrt{(\ell_1 + x_p)^2 + (y - y_p)^2} \tag{4.19}$$

$$= B_{p,K_3-1} - \Omega_{K_3-1}I_6\left(y_p - d, \ell_1 + x_p, \sqrt[3]{y_{K_3-1} - d}\right) \tag{4.20}$$

Thus, one gets

$$a_{p,K_3-1}^{(K_3-1)} = -I_6\left(y_p - d, \ell_1 + x_p, \sqrt[3]{y_{K_3-1} - d}\right) \tag{4.21}$$

to be used as a replacement to what was found using the traditional method. Ω_{K_3-1} is excluded from the system in the modified BEM.

On Segment DD_2 (from node $K_3 + 1$ to $K_3 + 2$),

$y = -x - \ell_1 + d,\ \theta = -\dfrac{\pi}{4},\ r = \sqrt{2}(x + \ell_1),\ \dfrac{\partial r}{\partial y} = \dfrac{y - d}{r},\ \dfrac{\partial\theta}{\partial y} = \dfrac{x + \ell_1}{r^2},\ \dfrac{\partial r}{\partial x} = \dfrac{x + \ell_1}{r},\ \dfrac{\partial\theta}{\partial x} = \dfrac{d - y}{r^2}$,

40

and $\dfrac{\partial \phi}{\partial n} = -\dfrac{1}{\sqrt{2}}\dfrac{\partial \phi}{\partial x} - \dfrac{1}{\sqrt{2}}\dfrac{\partial \phi}{\partial y}$ from Eq.(4.15) we get

$$-\frac{1}{\sqrt{2}}\frac{\partial \phi}{\partial x} = \frac{1}{2}\left(\frac{4}{3}M_4 \sqrt[6]{2}\sqrt[3]{x + \ell_1}\right) \tag{4.22}$$

and

$$-\frac{1}{\sqrt{2}}\frac{\partial \phi}{\partial y} = \frac{1}{2}\left(\frac{4}{3}M_4 \sqrt[6]{2}\sqrt[3]{x + \ell_1}\right) \tag{4.23}$$

Thus, adding Eq.(4.22) and Eq.(4.23) results in

$$\Omega = \frac{\partial \phi}{\partial n} = \frac{4M_4}{3}\sqrt[6]{2}\sqrt[3]{x + \ell_1} \tag{4.24}$$

At D_2, $x = x_{K_3+2}$, so

$$\Omega_{K_3+2} = \frac{4M_4}{3}\sqrt[6]{2}\sqrt[3]{x_{K_3+2} + \ell_1} \implies M_4 = \frac{3}{4\sqrt[6]{2}}\frac{\Omega_{K_3+2}}{\sqrt[3]{x_{K_3+2} + \ell_1}} \tag{4.25}$$

Therefore,

$$\Omega = \frac{\partial \phi}{\partial n} = \Omega_{K_3+2}\sqrt[3]{\frac{x + \ell_1}{x_{K_3+2} + \ell_1}} \tag{4.26}$$

Using Eq.(4.26), Eq.(2.7) becomes

$$I_{K_3+1,K_3+2}^{(p)} = B_{p,K_3+1} - \frac{\Omega_{K_3+2}}{\sqrt{2}}\int_{y_{K_3+1}}^{y_{K_3+2}}\sqrt[3]{\frac{x + \ell_1}{x_{K_3+2} + \ell_1}}\ln\left((x + x_p)^2 + (-x - \ell_1 + d - y_p)^2\right)dx \tag{4.27}$$

$$=B_{p,K_3+1} - \frac{\Omega_{K_3+3}\ln 8}{4\sqrt{2}}\left(x_{K_3+2} + \ell_1\right) \tag{4.28}$$

$$- \sqrt{2}\Omega_{K_3+2}I_6\left(\frac{x_p + \ell_1 - y_p + d}{2}, \frac{x_p + \ell_1 + y_p - d}{2}, \sqrt[3]{x_{K_3+2} + \ell_1}\right) \tag{4.29}$$

41

Thus, one gets

$$a_{p,K_3+2}^{(K_3+2)} = -\frac{\ln 8}{4\sqrt{2}}\left(x_{K_3+2} + \ell_1\right) - \sqrt{2}I_6\left(\frac{x_p + \ell_1 - y_p + d}{2}, \frac{x_p + \ell_1 + y_p - d}{2}, \sqrt[3]{x_{K_3+2} + \ell_1}\right) \quad (4.30)$$

to be used as a replacement to what was found using the traditional method. Ω_{K_3+1} is excluded from the system in the modified BEM.

4.3   Treatment of the Singularity at Point E

The local behavior around the singular point E is found. We consider the infinite extension of the segments adjacent to point E in Figure 2.1 preserving the boundary conditions, shown in Figure 4.7. The corresponding domain in the complex potential plane of the domain in Figure 4.7 is shown in Figure 4.8.

Figure 4.7:   Extension of Boundary Near Point E
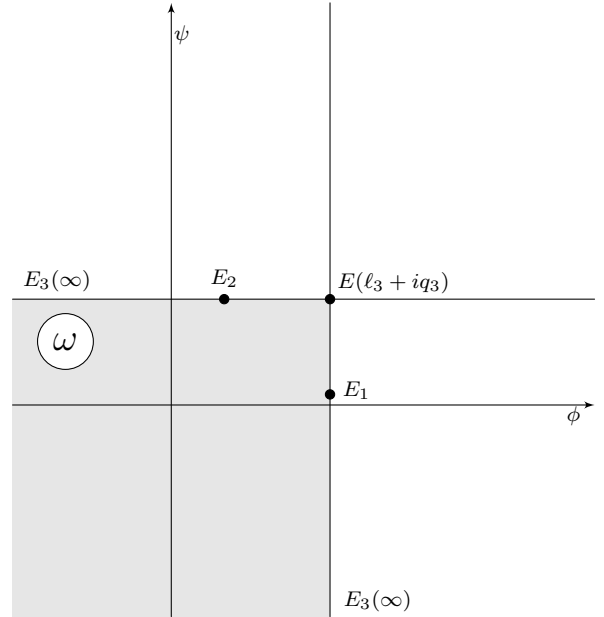
Figure 4.8:   Domain in Complex Potential Plane of Figure 4.7

42

The conformal mapping that maps the domain in Figure 4.7 to the corresponding domain Figure 4.8 is

$$\omega = -\sqrt{\frac{M_5^*(z - (-R + i\kappa))^4}{(z - i(\kappa - R))^4 - (z - (-R + i\kappa))^4}} + \ell_3 + q_3 i \tag{4.31}$$

where $M_5^* > 0$ and q_3 are arbitrary real numbers. Using Eq.(4.31) and choosing any M_5 and q_3 results in the the flow net in Figure 4.9. Since $\omega = \phi + i\psi$, $\phi(x, y)$ is the real part of ω. Thus, it can be shown that if

$$f_1(x, y) = x^2 + (y - \kappa)^2 \tag{4.32}$$

$$f_2(x, y) = 2R(R - \kappa + x + y) \tag{4.33}$$

$$f_3(x, y) = f_1(x, y) + f_2(x, y) \tag{4.34}$$

$$f_4(x, y) = 2f_1(x, y) + f_2(x, y) - R^2 \tag{4.35}$$

$$f(x, y) = \frac{(x + r)^2 + (y - \kappa)^2}{2\sqrt{R^2 f_1(x, y) f_3(x, y) f_4(x, y)}} \tag{4.36}$$

and

$$g(x, y) = \cos\left(\frac{1}{2}\mathrm{Arg}\left(\frac{M_5^*(x + iy - (i\kappa - R))^4}{(x + iy - i(\kappa - R))^4 - (x + iy - i(\kappa - R))^4}\right)\right), \tag{4.37}$$

then we get

$$\phi(x, y) = \ell_3 - M_5 f(x, y) \cdot g(x, y), \tag{4.38}$$

where $M_5 = \sqrt{5M_5^*}$, as the solution of the BVP for the domain in Figure 4.7.

On Segment E_1E (from node $K_4 - 1$ to K_4),
$y = -x - \ell_2 - 2R$, $\dfrac{\partial \phi}{\partial n} = -\dfrac{1}{\sqrt{2}}\dfrac{\partial \phi}{\partial x} - \dfrac{1}{\sqrt{2}}\dfrac{\partial \phi}{\partial y}$ from Eq.4.38, we can get

$$\Omega = \frac{\partial \phi}{\partial n} = -\frac{1}{\sqrt{2}}\frac{\partial \phi}{\partial x} - \frac{1}{\sqrt{2}}\frac{\partial \phi}{\partial y} = -\frac{M_5}{\sqrt{2}}\left(\frac{\partial \phi}{\partial x}(x, -x - \ell_2 - 2R) + \frac{\partial \phi}{\partial y}(x, -x - \ell_2 - 2R)\right) \tag{4.39}$$

43
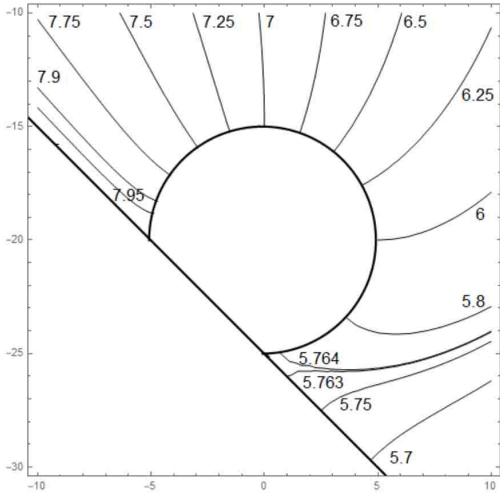
(a) Contour plot for various values of ϕ
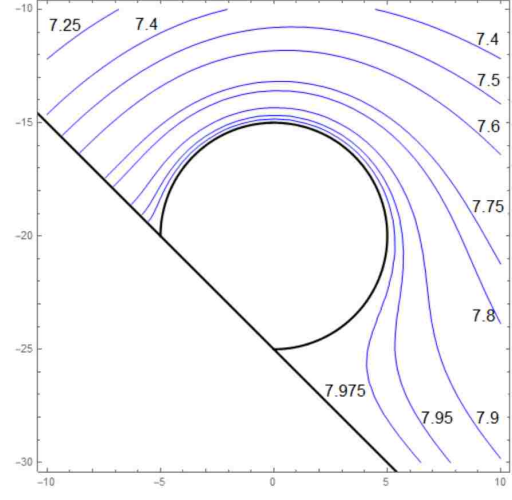
(b) Contour plot for various values of ψ
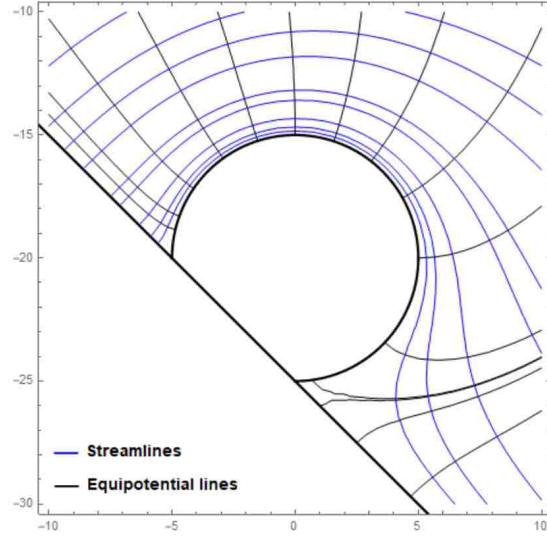
(c) Flownet of Domain in Figure 4.7

Figure 4.9: Contour Plots of Domain in Figure 4.7

At E_1, $x = x_{K_4-1}$, so

$$\Omega_{K_4-1} = -\frac{M_5}{\sqrt{2}}\left(\frac{\partial\phi}{\partial x}(x_{K_4-1}, -x_{K_4-1} - \ell_2 - 2R) + \frac{\partial\phi}{\partial y}(x_{K_4-1}, -x_{K_4-1} - \ell_2 - 2R)\right) \qquad (4.40)$$

Thus,

$$M_5 = -\sqrt{2}\Omega_{K_4-1}\left(\frac{\partial\phi}{\partial x}(x_{K_4-1}, -x_{K_4-1}-\ell_2-2R) + \frac{\partial\phi}{\partial y}(x_{K_4-1}, -x_{K_4-1}-\ell_2-2R)\right)^{-1} \quad (4.41)$$

Therefore,

$$\Omega = \Omega_{K_4-1}\frac{\left(\frac{\partial\phi}{\partial x}(x, -x-\ell_2-2R) + \frac{\partial\phi}{\partial y}(x, -x-\ell_2-2R)\right)}{\left(\frac{\partial\phi}{\partial x}(x_{K_4-1}, -x_{K_4-1}-\ell_2-2R) + \frac{\partial\phi}{\partial y}(x_{K_4-1}, -x_{K_4-1}-\ell_2-2R)\right)}. \quad (4.42)$$

Let $\zeta = \left(\frac{\partial\phi}{\partial x}(x_{K_4-1}, -x_{K_4-1}-\ell_2-2R) + \frac{\partial\phi}{\partial y}(x_{K_4-1}, -x_{K_4-1}-\ell_2-2R)\right)$. Using Eq.(4.42), Eq.(2.7)

becomes

$$I^{(p)}_{K_4-1,K_4} = B_{p,K_4-1} - \frac{\Omega_{K_4-1}}{\zeta}\int_{x_{K_4-1}}^{x_{K_4}}\left(\frac{\partial\phi}{\partial x}(x, -x-\ell_2-2R) + \frac{\partial\phi}{\partial y}(x, -x-\ell_2-2R)\right)\ln(r_p)\, dx$$

$$= B_{p,K_4-1} - \Omega_{K_4-1}I_8\left(x_{K_4-1}, x_{K_4}, x_p - \frac{1}{2}s_p, \frac{s_p}{2}\right) \quad (4.43)$$

Thus, one gets

$$a^{(K_4-1)}_{p,K_4-1} = -I_8\left(x_{K_4-1}, x_{K_4}, x_p - \frac{1}{2}s_p, \frac{s_p}{2}\right) \quad (4.44)$$

to be used as a replacement to what was found using the traditional method. Ω_{K_4} is excluded from the system in the modified BEM.

On Segment EE_2 (from node K_4+1 to K_4+2),
$x^2 + (\kappa+y)^2 = R^2$, $x = R\cos\theta$, and $y = R\sin\theta - \kappa$. Hence

$$\Omega = \phi(x,y) = \ell_3 - M_5 f(x,y) \cdot g(x,y) \quad (4.45)$$

45

where now

$$f(R\cos\theta, R\sin\theta - \kappa) = \hat{f}(\theta) = \frac{1 + \cos\theta}{\sqrt{3 + 2(\cos\theta + \sin\theta)}} \tag{4.46}$$

and

$$g(R\cos\theta, R\sin\theta - \kappa) = \hat{g}(\theta) = \cos\left(\frac{1}{2}\arg\left(\frac{M_5^*}{4e^{2i\theta}(2\sin\theta + 2\cos\theta + 3)}\right)\right) \tag{4.47}$$

At E_2, $\theta = \theta_{K_4+2}$, so

$$\Omega_{K_4+2} = \ell_3 - M_5\hat{f}(\theta_{K_4+2})\hat{g}(\theta_{K_4+2}) \tag{4.48}$$

Thus

$$M_5 = \frac{\ell_3 - \Omega_{K_4+2}}{\hat{f}(\theta_{K_4+2})\hat{g}(\theta_{K_4+2})} \tag{4.49}$$

Therefore,

$$\Omega = \phi = \ell_3 + \left(\frac{\Omega_{K_4+2} - \ell_3}{\hat{f}(\theta_{K_4+2})\hat{g}(\theta_{K_4+2})}\right)\hat{f}(\theta)\hat{g}(\theta) \tag{4.50}$$

Using Eq.(4.50), Eq.(2.7) becomes

$$I_{K_4+1,K_4+2}^{(p)} = \int_{\theta_{K_4+1}}^{\theta_{K_4+2}} \left(\left(\frac{\hat{f}(\theta)\hat{g}(\theta)}{\hat{f}(\theta_{K_4+2})\hat{g}(\theta_{K_4+2})}\right)\Omega_{K_4+2} + \ell_3\left(1 - \frac{\hat{f}(\theta)\hat{g}(\theta)}{\hat{f}(\theta_{K_4+2})\hat{g}(\theta_{K_4+2})}\right)\right)\frac{r}{r_p}\frac{\partial r_p}{\partial n}\,d\theta \tag{4.51}$$

$$= \frac{\Omega_{K_4+2}}{\hat{f}(\theta_{K_4+2})\hat{g}(\theta_{K_4+2})}I_9(\theta_{K_4+1}, \theta_{K_4+2}, x_p, y_p - \kappa, R) + I_{10}(\theta_{K_4+1}, \theta_{K_4+2}, x_p, y_p - \kappa, R) \tag{4.52}$$

Thus, one gets

$$a_{p,K_4+2}^{(K_4+2)} = \frac{1}{\hat{f}(\theta_{K_4+2})\hat{g}(\theta_{K_4+2})}I_9(\theta_{K_4+1}, \theta_{K_4+2}, x_p, y_p - \kappa, R) \tag{4.53}$$

to be used as a replacement to what was found using the traditional method. Ω_{K_4+1} is excluded from the system in the modified BEM.

4.4 Treatment of the Singularity at Point F

The local behavior near the singular point F is found. We consider the infinite extension of the adjacent sides of point F in Figure 2.1 preserving the boundary conditions, shown in Figure 4.10. The corresponding domain in the complex potential plane of the domain in Figure 4.10 is shown Figure 4.11.
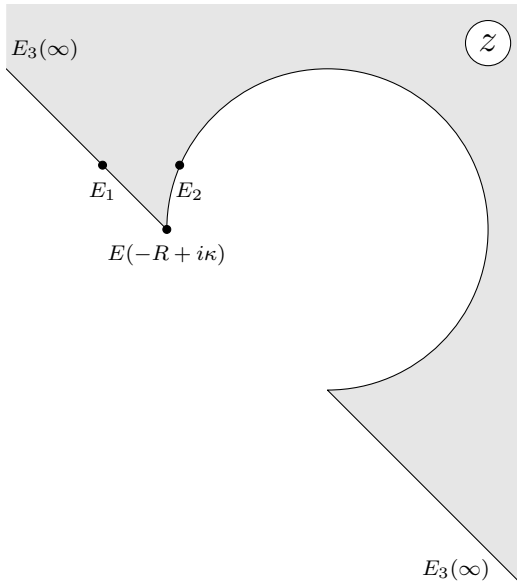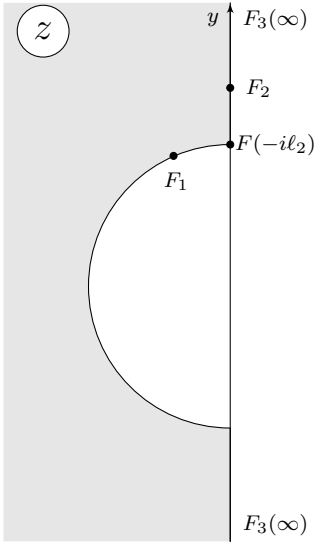

Figure 4.10: Extension of Boundary Near Point F
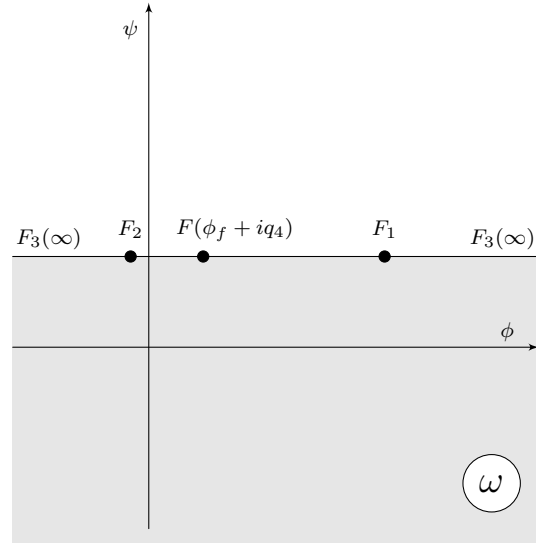
Figure 4.11: Domain in Complex Potential Plane of Figure 4.10

The conformal mapping that maps the domain in Figure 4.10 to the domain on Figure 4.11 is

$$\omega = -M_7 \frac{(z + i\ell_2)^2}{(z - i(\kappa - R))^2 - (z + i\ell_2)^2} + \phi_F + iq_4 \tag{4.54}$$

$$= -M_7 \frac{(z - i(\kappa + R))^2}{(z - i(\kappa - R))^2 - (z - i(\kappa + R))^2} + \phi_F + iq_4 \tag{4.55}$$

where q_4 and ϕ_f are arbitrary real numbers and $M_7 > 0$. Using Eq.(4.55) and any choice M_3 and q_2 results in the the flow net in Figure 4.12. Since $\omega = \phi + i\psi$, $\phi(x, y)$ is the real part of ω. Thus,

it can be shown that

$$\phi(x, y) = \phi_F + \frac{M_7}{4}\left(2 + \frac{\kappa - y}{R} + \frac{R(\kappa - y)}{x^2 + (\kappa - y)^2}\right), \tag{4.56}$$

where $\phi_F = \Omega_{K_5}$, is the solution of the BVP for the domain shown in Figure 4.10.
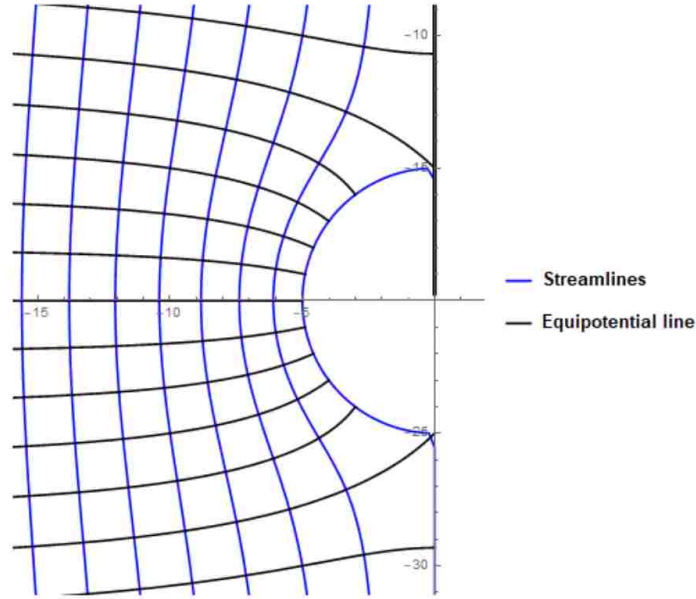
Figure 4.12: Flownet of Domain in Figure 4.10

On Segment F_1F (from node $K_5 - 1$ to K_5),

$x^2 + (y - \kappa)^2 = R^2$ and $y = R\sin\theta + \kappa$ hence

$$\Omega = \phi = \Omega_{K_5} + \frac{M_7}{2}(1 - \sin\theta) \tag{4.57}$$

At F_1, $\theta = \theta_{K_5-1}$, so

$$\Omega_{K_5-1} = \Omega_{K_5} + \frac{M_7}{2}\left(1 - \sin\theta_{K_5-1}\right) \implies M_7 = \frac{2(\Omega_{K_5-1} - \Omega_{K_5})}{\left(1 - \sin\theta_{K_5-1}\right)} \tag{4.58}$$

48

Therefore,

$$\Omega = \frac{\Omega_{K_5}(\sin\theta - \sin\theta_{K_{5-1}}) + \Omega_{K_{5-1}}(1 - \sin\theta)}{\left(1 - \sin\theta_{K_{5-1}}\right)} \tag{4.59}$$

Using Eq.(4.59), Eq.(2.7) becomes

$$\begin{aligned} I^{(p)}_{K_{5-1},K_5} = \int_{\theta_{K_{5-1}}}^{\theta_{K_5}} & \left(\frac{\Omega_{K_5}(\sin\theta - \sin\theta_{K_{5-1}}) + \Omega_{K_{5-1}}(1 - \sin\theta)}{\left(1 - \sin\theta_{K_{5-1}}\right)} \right) \cdot \\ & \frac{R^2 - x_p R\cos\theta - (y_p - \kappa)R\sin\theta}{(R\cos\theta - x_p)^2 + (R\sin\theta - (y_p - \kappa))^2} \, d\theta \end{aligned} \tag{4.60}$$

Thus, one gets

$$a^{(K_{5-1})}_{p,K_{5-1}} = \frac{1}{1 - \sin\left(\theta_{K_{5-1}}\right)} I_{11}(\theta_{K_{5-1}}, \theta_{K_5}, x_p, y_p - \kappa, R, 1) \tag{4.61}$$

to be used as a replacement to what was found using the traditional method. $a^{(K_5)}_{p,K_5}$ will be given later on in this section.

On Segment FF_2 (from node K_5 to $K_5 + 1$),

$x = 0$. From Eq.(4.56) we get

$$\phi = \Omega_{K_5} + \frac{M_8}{4}\left(2 + \frac{k - y}{R} + \frac{R(k - y)}{x^2 + (k - y)^2}\right) = \Omega_{K_5} + \frac{M_8}{4}\left(2 + \frac{k - y}{R} + \frac{R}{k - y}\right) \tag{4.62}$$

At F_2, $y = y_{K_5+1}$, so

$$\Omega_{K_5+1} = \Omega_{K_5} + \frac{M_8}{4}\left(2 + \frac{k - y_{K_5+1}}{R} + \frac{R}{k - y_{K_5+1}}\right) \implies \tag{4.63}$$

$$M_8 = \frac{4(\Omega_{K_5+1} - \Omega_{K_5})}{2 + \frac{k - y_{K_5+1}}{R} + \frac{R}{k - y_{K_5+1}}} = \frac{4R(k - y_{K_5+1})(\Omega_{K_5+1} - \Omega_{K_5})}{2R(k - y_{K_5+1}) + (k - y_{K_5+1})^2 + R^2} \tag{4.64}$$

49

Therefore,

$$\Omega = \Omega_{K_5} + \frac{R(k - y_{K_5+1})(\Omega_{K_5+1} - \Omega_{K_5})}{(R + (\kappa - y_{K_5+1}))^2}\left(2 + \frac{k - y}{R} + \frac{R}{k - y}\right) \tag{4.65}$$

Using Eq.(4.65), Eq.(2.7) becomes

$$
\begin{aligned}
I^{(p)}_{K_5, K_5+1} = {} & -\Omega_{K_5} \int_{y_{K_5}}^{y_{K_5+1}} \frac{x_p}{x_p^2 + (y - y_p)^2}\, dy \\
& - \frac{R(\kappa - y_{K_5+1})(\Omega_{K_5+1} - \Omega_{K_5})}{(R + (\kappa - y_{K_5+1}))^2} \int_{y_{K_5}}^{y_{K_5+1}} \frac{2x_p}{x_p^2 + (y - y_p)^2}\, dy \\
& - \frac{R(\kappa - y_{K_5+1})(\Omega_{K_5+1} - \Omega_{K_5})}{(R + (\kappa - y_{K_5+1}))^2} \int_{y_{K_5}}^{y_{K_5+1}} \frac{(\kappa - y)x_p}{R((x_p)^2 + (y - y_p)^2)}\, dy \\
& - \frac{R(\kappa - y_{K_5+1})(\Omega_{K_5+1} - \Omega_{K_5})}{(R + (\kappa - y_{K_5+1}))^2} \int_{y_{K_5}}^{y_{K_5+1}} \frac{Rx_p}{(\kappa - y)((x_p)^2 + (y - y_p)^2)}\, dy \tag{4.66}
\end{aligned}
$$

Let

$$\xi = \frac{R(\kappa - y_{K_5+1})}{(R + (\kappa - y_{K_5+1}))^2} \tag{4.67}$$

Then, Eq.(4.66) becomes

$$
\begin{aligned}
I^{(p)}_{K_5, K_5+1} = {} & -\Omega_{K_5} I_3(y_{K_5}, y_{K_5+1}, y_p, x_p) \\
& - 2\xi(\Omega_{K_5+1} - \Omega_{K_5}) I_3(y_{K_5}, y_{K_5+1}, y_p, x_p) \\
& + \frac{x_p \xi}{r}(\Omega_{K_5+1} - \Omega_{K_5})\left(\ln\left|\sqrt{\frac{(y_{K_5+1} - y_p)^2 + + x_p^2}{(y_{K_5} - y_p)^2 + x_p^2}}\right| + \frac{y_p - \kappa}{x_p} I_3(y_{K_5}, y_{K_5+1}, y_p, x_p)\right) \\
& + R\xi(\Omega_{K_5+1} - \Omega_{K_5}) I_{12}(y_{K_5}, y_{K_5+1}, y_p, x_p, \kappa) \tag{4.68}
\end{aligned}
$$

50

Let

$$\eta = \sqrt{\frac{(y_{K_5+1} - y_p)^2 + + x_p^2}{(y_{K_5} - y_p)^2 + x_p^2}} \tag{4.69}$$

Then, Eq.(4.68) becomes

$$\left(\frac{x_p}{r} \ln |\eta| + \left(\frac{y_p - \kappa}{R} - 2\right) I_3 + r I_{12}\right) \xi \Omega_{K_5+1} - \left(\frac{x_p}{R} \ln |\eta| + \left(\frac{y_p - \kappa}{R} - 2 - \frac{1}{\xi}\right) I_3 + R I_{12}\right) \xi \Omega_{K_5} \tag{4.70}$$

Thus, one gets

$$a_{p,K_5}^{(K_5)} = -\left(\frac{x_p}{R} \ln |\eta| + \left(\frac{y_p - \kappa}{R} - 2 - \frac{1}{\xi}\right) I_3 + R I_{12}\right) \xi$$

$$- (1 - \sin(\theta_{K_{5-1}}))^{-1} I_{11}(\theta_{K_{5-1}}, \theta_{K_5}, x_p, y_p - \kappa, \sin(\theta_{K_{5-1}}), R) \tag{4.71}$$

$$a_{p,K_5+1}^{(K_5+1)} = \left(\frac{x_p}{R} \ln |\eta| + \left(\frac{y_p - \kappa}{R} - 2\right) I_3 + R I_{12}\right) \xi \tag{4.72}$$

to be used as replacements to what was found using the traditional method.

CHAPTER 5

CONCLUSIONS

5.1 Numerical Results

Both the Traditional and Modified BEM were implemented in programs using Mathematica 11 (Wolfram Research Inc. 2018). The program asks for the following dimensions to construct a domain like in Figure 2.11: ℓ_1, ℓ_2, ℓ_3, and R. One must be cautious when inputing these values, since d is calculated by finding the intersection of the lines $x = -\ell_1$ and $y = -x - (\ell_2 - 2R)$. $d < \ell_3$ is imposed to insure a simply connected domain without any self-intersections. The dimensions used for the results in this section are $\ell_1 = 20$, $\ell_2 = 15$, $\ell_3 = 8$, and $R = 5$. The amount of boundary elements used for the BEM and modified BEM are as follows: $k_1 = 14$, $k_7 = 5$, $k_2 = 135$, $k_8 = 1$, $k_3 = 40$, $k_4 = 69$, $k_5 = 45$, $k_6 = 50$. In the first iteration of both the BEM and
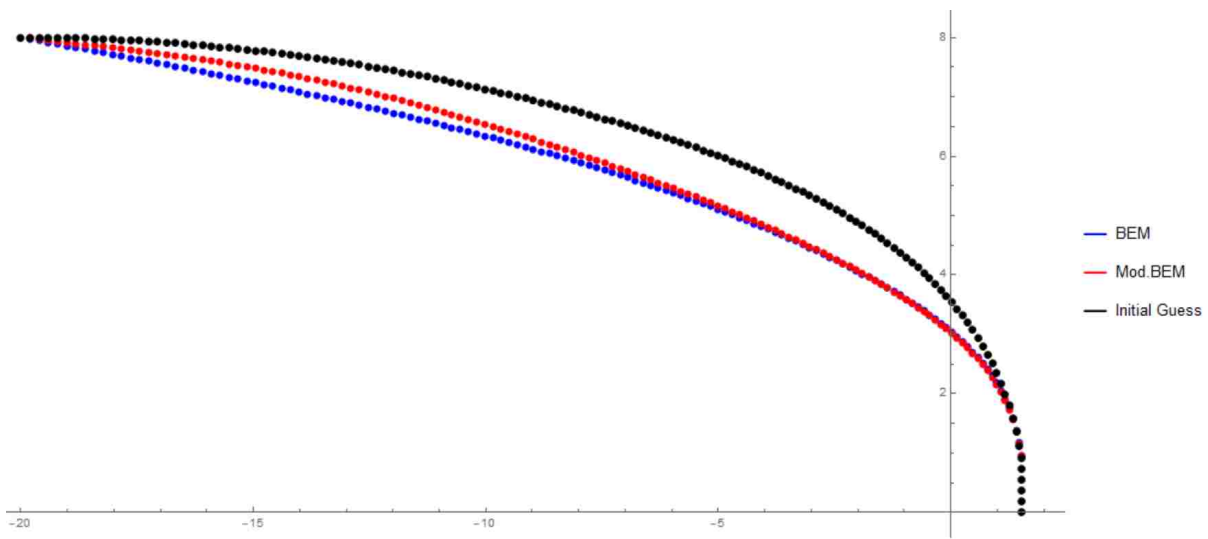
Figure 5.1: First Iteration at $b' = 1.515$
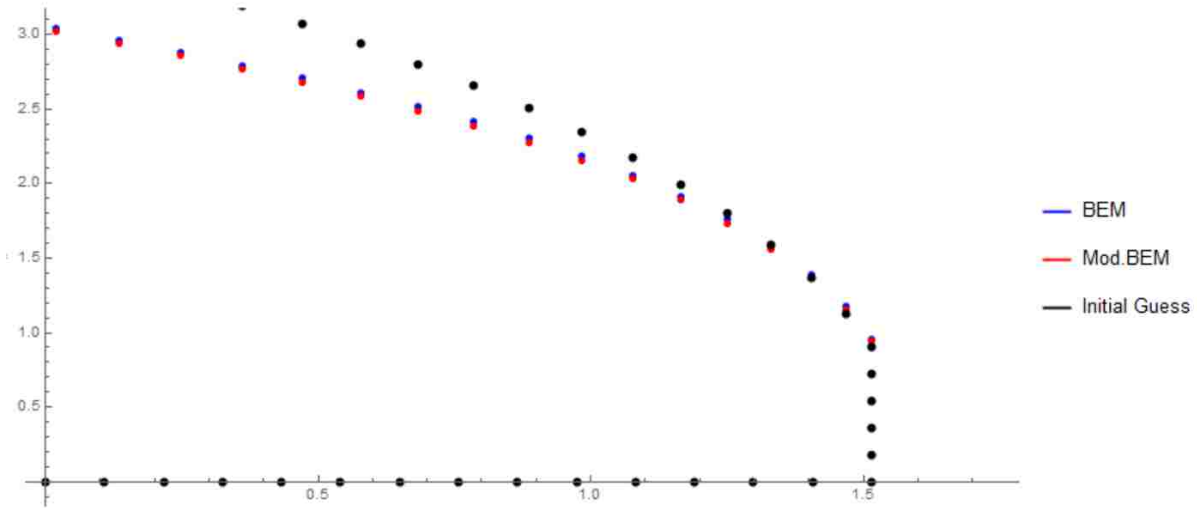
Figure 5.2: View of Exit Point in Figure 5.1

Modified BEM have similar results with both appearing to be correct. This is shown in Figures 5.1 and Figures 5.2. Let $\Omega_m^{(1)}$ be the results from the traditional BEM and $\Omega_m^{(2)}$ be the results from the modified BEM. The data for the first iteration can be seen in Table 5.1.

m	x_m	y_m	$\Omega_m^{(1)}$	$\Omega_m^{(2)}$	$\left|y_m - \Omega_m^{(1)}\right|$		$\left|y_m - \Omega_m^{(2)}\right|$
19	1.515	0.906	0.953	0.946	0.047		0.04
20	1.468	1.123	1.18	1.152	0.057		0.029
21	1.404	1.364	1.39	1.365	0.026		0.001
22	1.33	1.589	1.584	1.56	0.005		0.029
23	1.251	1.799	1.758	1.734	0.041		0.065
24	1.165	1.993	1.913	1.889	0.08		0.104
25	1.076	2.175	2.054	2.03	0.121		0.145
26	0.983	2.345	2.183	2.158	0.163		0.187
27	0.886	2.506	2.301	2.277	0.205		0.229
28	0.786	2.658	2.411	2.387	0.247		0.27
29	0.684	2.802	2.514	2.491	0.288		0.311
30	0.578	2.939	2.612	2.589	0.327		0.35
31	0.471	3.07	2.704	2.682	0.366		0.388
32	0.361	3.195	2.792	2.771	0.403		0.424
33	0.249	3.315	2.877	2.856	0.438		0.459
34	0.135	3.43	2.958	2.938	0.472		0.492
35	0.019	3.541	3.036	3.018	0.504		0.523

m	x_m	y_m	$\Omega_m^{(1)}$	$\Omega_m^{(2)}$	$\left| y_m - \Omega_m^{(1)} \right|$	$\left| y_m - \Omega_m^{(2)} \right|$
36	-0.099	3.647	3.112	3.095	0.535	0.553
37	-0.218	3.75	3.186	3.17	0.564	0.58
38	-0.34	3.849	3.258	3.243	0.591	0.607
39	-0.462	3.945	3.328	3.314	0.617	0.631
40	-0.587	4.038	3.396	3.384	0.642	0.654
41	-0.713	4.128	3.464	3.452	0.665	0.676
42	-0.84	4.215	3.529	3.52	0.686	0.696
43	-0.969	4.3	3.594	3.586	0.706	0.715
44	-1.099	4.382	3.657	3.651	0.725	0.732
45	-1.23	4.462	3.72	3.715	0.742	0.748
46	-1.363	4.54	3.781	3.778	0.759	0.762
47	-1.496	4.616	3.842	3.84	0.774	0.776
48	-1.631	4.69	3.902	3.902	0.788	0.788
49	-1.768	4.762	3.961	3.963	0.801	0.799
50	-1.905	4.832	4.019	4.023	0.813	0.81
51	-2.043	4.901	4.077	4.082	0.824	0.819
52	-2.183	4.968	4.133	4.141	0.834	0.827
53	-2.324	5.033	4.19	4.199	0.844	0.834
54	-2.465	5.097	4.245	4.257	0.852	0.841
55	-2.608	5.16	4.3	4.314	0.86	0.846
56	-2.752	5.221	4.354	4.37	0.867	0.851
57	-2.896	5.281	4.408	4.426	0.873	0.855
58	-3.042	5.34	4.461	4.482	0.879	0.858
59	-3.188	5.397	4.514	4.537	0.884	0.86
60	-3.336	5.454	4.566	4.592	0.888	0.862
61	-3.484	5.509	4.617	4.646	0.892	0.863
62	-3.633	5.563	4.669	4.699	0.895	0.864
63	-3.783	5.617	4.719	4.753	0.898	0.864
64	-3.934	5.669	4.769	4.806	0.9	0.863
65	-4.086	5.72	4.819	4.858	0.902	0.862
66	-4.239	5.771	4.868	4.91	0.903	0.861
67	-4.392	5.82	4.917	4.962	0.904	0.859
68	-4.546	5.869	4.965	5.013	0.904	0.856
69	-4.701	5.917	5.013	5.064	0.904	0.853
70	-4.857	5.964	5.06	5.115	0.904	0.849
71	-5.014	6.01	5.107	5.165	0.904	0.845
72	-5.171	6.056	5.153	5.215	0.903	0.841
73	-5.329	6.101	5.199	5.265	0.901	0.836
74	-5.488	6.145	5.245	5.314	0.9	0.831
75	-5.647	6.189	5.29	5.363	0.898	0.826
76	-5.808	6.231	5.335	5.411	0.896	0.82

m	x_m	y_m	$\Omega_m^{(1)}$	$\Omega_m^{(2)}$	$\left|y_m - \Omega_m^{(1)}\right|$		$\left|y_m - \Omega_m^{(2)}\right|$	
77	-5.969	6.274	5.38	5.46	0.894		0.814	
78	-6.13	6.315	5.424	5.508	0.891		0.807	
79	-6.293	6.356	5.468	5.556	0.889		0.801	
80	-6.456	6.397	5.511	5.603	0.886		0.793	
81	-6.619	6.436	5.554	5.65	0.883		0.786	
82	-6.784	6.476	5.597	5.697	0.879		0.778	
83	-6.948	6.515	5.639	5.744	0.876		0.77	
84	-7.114	6.553	5.681	5.79	0.872		0.762	
85	-7.28	6.59	5.722	5.837	0.868		0.754	
86	-7.447	6.628	5.763	5.883	0.864		0.745	
87	-7.615	6.664	5.804	5.928	0.86		0.736	
88	-7.783	6.701	5.845	5.974	0.856		0.727	
89	-7.952	6.736	5.885	6.019	0.852		0.718	
90	-8.121	6.772	5.925	6.064	0.847		0.708	
91	-8.291	6.807	5.964	6.108	0.842		0.698	
92	-8.461	6.841	6.004	6.153	0.838		0.688	
93	-8.633	6.875	6.043	6.197	0.833		0.678	
94	-8.804	6.909	6.081	6.241	0.828		0.668	
95	-8.977	6.942	6.119	6.284	0.823		0.658	
96	-9.149	6.975	6.157	6.328	0.818		0.647	
97	-9.323	7.008	6.195	6.371	0.813		0.637	
98	-9.497	7.04	6.232	6.414	0.807		0.626	
99	-9.671	7.071	6.27	6.456	0.802		0.615	
100	-9.846	7.103	6.306	6.498	0.796		0.605	
101	-10.022	7.133	6.343	6.54	0.791		0.594	
102	-10.198	7.164	6.379	6.581	0.785		0.582	
103	-10.375	7.194	6.415	6.622	0.779		0.571	
104	-10.552	7.223	6.451	6.663	0.772		0.56	
105	-10.73	7.252	6.486	6.703	0.766		0.549	
106	-10.908	7.28	6.521	6.743	0.759		0.537	
107	-11.087	7.308	6.556	6.783	0.753		0.526	
108	-11.266	7.336	6.591	6.822	0.745		0.514	
109	-11.446	7.363	6.625	6.86	0.738		0.503	
110	-11.626	7.39	6.659	6.898	0.731		0.491	
111	-11.807	7.416	6.693	6.936	0.723		0.48	
112	-11.988	7.441	6.727	6.973	0.715		0.468	
113	-12.17	7.466	6.76	7.009	0.706		0.457	
114	-12.352	7.491	6.793	7.045	0.698		0.446	
115	-12.535	7.515	6.826	7.081	0.689		0.434	
116	-12.718	7.538	6.859	7.115	0.679		0.423	
117	-12.901	7.561	6.892	7.149	0.67		0.412	

m	x_m	y_m	$\Omega_m^{(1)}$	$\Omega_m^{(2)}$	$\left\lvert y_m - \Omega_m^{(1)} \right\rvert$	$\left\lvert y_m - \Omega_m^{(2)} \right\rvert$
118	-13.086	7.584	6.924	7.183	0.66	0.401
119	-13.27	7.606	6.956	7.216	0.65	0.39
120	-13.455	7.627	6.988	7.248	0.639	0.379
121	-13.641	7.648	7.02	7.279	0.628	0.369
122	-13.827	7.668	7.052	7.31	0.617	0.358
123	-14.013	7.688	7.083	7.34	0.605	0.348
124	-14.2	7.707	7.115	7.37	0.593	0.338
125	-14.387	7.726	7.146	7.398	0.58	0.328
126	-14.575	7.744	7.177	7.426	0.567	0.318
127	-14.763	7.761	7.208	7.453	0.554	0.308
128	-14.952	7.778	7.238	7.48	0.54	0.298
129	-15.141	7.794	7.269	7.506	0.525	0.289
130	-15.33	7.81	7.3	7.531	0.511	0.279
131	-15.52	7.825	7.33	7.556	0.495	0.27
132	-15.711	7.84	7.36	7.58	0.48	0.26
133	-15.901	7.854	7.39	7.603	0.463	0.251
134	-16.092	7.867	7.42	7.626	0.447	0.242
135	-16.284	7.88	7.45	7.648	0.43	0.232
136	-16.476	7.892	7.48	7.669	0.412	0.223
137	-16.668	7.903	7.51	7.69	0.394	0.213
138	-16.861	7.914	7.54	7.711	0.375	0.203
139	-17.055	7.924	7.569	7.731	0.355	0.193
140	-17.248	7.934	7.599	7.751	0.335	0.183
141	-17.442	7.943	7.628	7.77	0.315	0.173
142	-17.637	7.951	7.657	7.789	0.294	0.162
143	-17.831	7.959	7.687	7.808	0.272	0.151
144	-18.027	7.966	7.716	7.826	0.25	0.14
145	-18.222	7.972	7.745	7.844	0.227	0.128
146	-18.418	7.978	7.774	7.862	0.204	0.116
147	-18.615	7.983	7.803	7.88	0.18	0.103
148	-18.811	7.988	7.832	7.898	0.155	0.09
149	-19.009	7.991	7.861	7.915	0.13	0.076
150	-19.206	7.995	7.89	7.932	0.104	0.062
151	-19.404	7.997	7.919	7.95	0.078	0.047
152	-19.602	7.999	7.948	7.967	0.051	0.031
153	-19.801	8.	7.977	7.986	0.023	0.014

Table 5.1: Results of First Iteration

Now if we plot the nodes for the phreatic surface for the first 51 iterations we get Figure 5.4 for the Modified BEM and Figure 5.3 fo the Traditional BEM. The figures are color coded with the later the iteration the lighter the color.
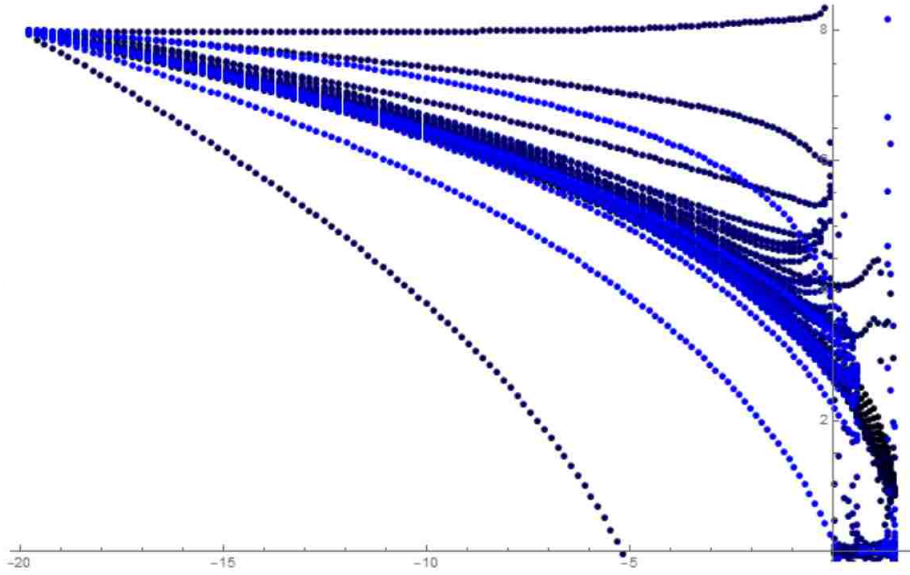
Figure 5.3: 51 Iteration at $b' = 1.515$ with Traditional BEM

From Figures 5.4, 5.5, and 5.3 the conclusion that the Modified BEM is improving the stability for the numerical solution is clear. Now, Figure 5.3 is a slight exaggeration, in that it is very visually impactful, but in a more efficient program than my own, the iteration would have just

Figure 5.4: 51 Iteration at $b' = 1.515$ with Modified BEM

been terminated on the 31st loop when node $\Omega_{K_7} < 0$ first occurred. Nevertheless, the results stand and after 51 iterations we arrive at Figure 5.6 and Table 5.2
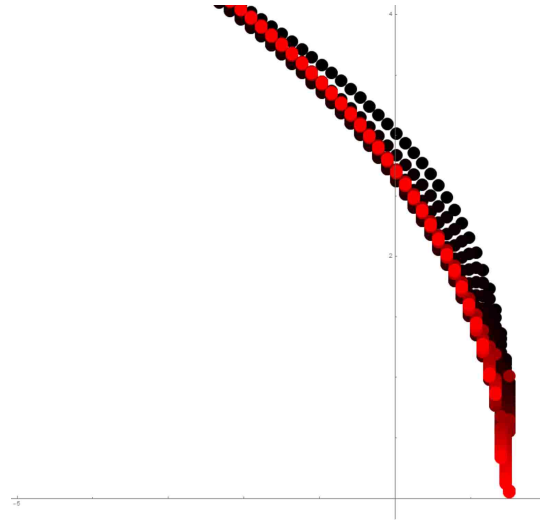
Figure 5.5: View of Exit Point in Figure 5.4
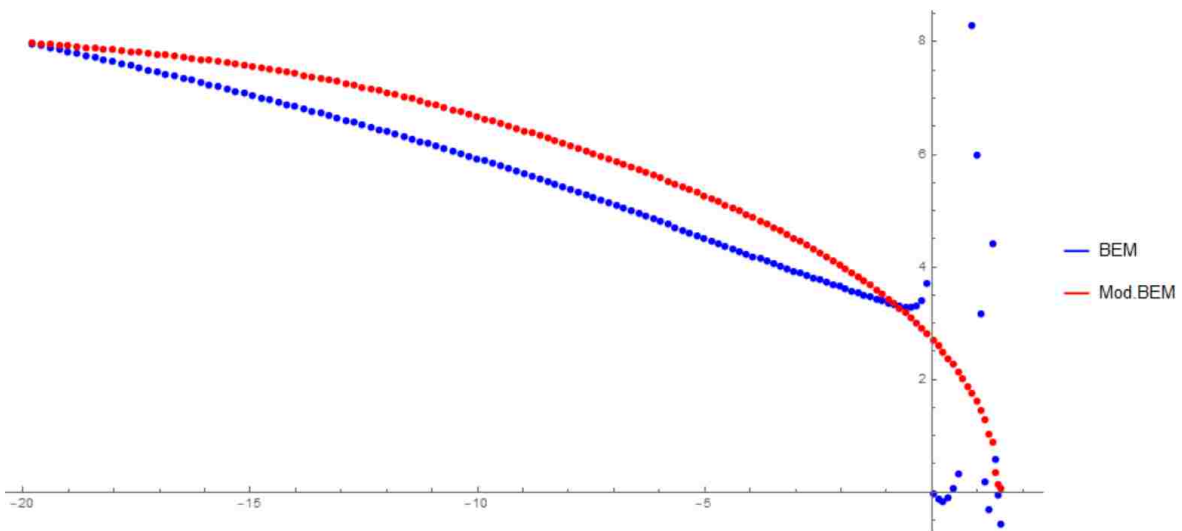
Figure 5.6: 51st Iteration at $b' = 1.515$

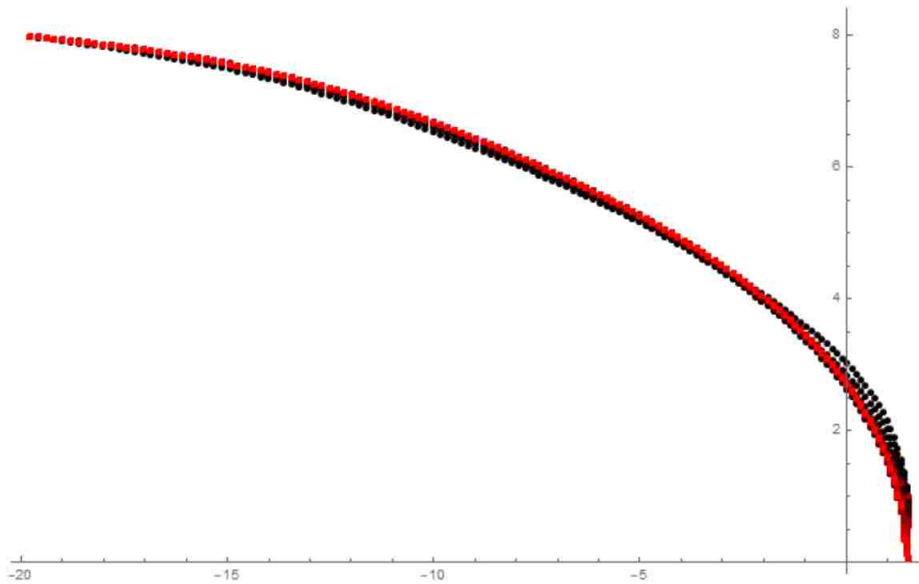| m	x_m	$\Omega_m^{(1)}$	$\Omega_m^{(2)}$	$\left\|y_m^{(50)} - \Omega_m^{(1)}\right\|$		$\left\|y_m^{(50)} - \Omega_m^{(2)}\right\|$
19	1.515	-0.571	0.053	0.46983		0.00102
20	1.468	-0.046	0.123	190.722		0.01638
21	1.404	0.568	0.337	55.244		0.0055
22	1.33	4.417	0.875	27.327		0.00496
23	1.251	-0.308	1.033	0.31607		0.00587
24	1.165	0.178	1.278	0.14859		0.00563
25	1.076	3.176	1.45	2.49626		0.00096
26	0.983	5.98	1.604	4.4521		0.00111
27	0.886	8.295	1.747	5.79722		0.00137
28	0.786	10.178	1.884	6.84976		0.00108
29	0.684	12.865	2.016	8.39369		0.00079
30	0.578	0.312	2.141	0.10532		0.00056
31	0.471	0.073	2.262	0.2264		0.00039
32	0.361	-0.094	2.378	0.17508		0.00028
33	0.249	-0.172	2.489	0.07154		0.0002
34	0.135	-0.132	2.597	0.02123		0.00015
35	0.019	-0.039	2.701	0.05475		0.00011
36	-0.099	3.714	2.802	4.87508		0.00009
37	-0.218	3.404	2.9	4.35361		0.00007
38	-0.34	3.315	2.996	4.10379		0.00006
39	-0.462	3.288	3.088	3.96464		0.00006
40	-0.587	3.291	3.178	3.8781		0.00005
41	-0.713	3.308	3.266	3.81083		0.00005
42	-0.84	3.333	3.352	3.75339		0.00005
43	-0.969	3.363	3.436	3.70183		0.00004
44	-1.099	3.396	3.518	3.65409		0.00004
45	-1.23	3.43	3.598	3.60889		0.00004
46	-1.363	3.466	3.677	3.56538		0.00004
47	-1.496	3.502	3.754	3.52293		0.00004
48	-1.631	3.539	3.829	3.48105		0.00004
49	-1.768	3.576	3.903	3.4394		0.00004
50	-1.905	3.614	3.976	3.39771		0.00004
51	-2.043	3.651	4.047	3.35583		0.00004
52	-2.183	3.689	4.117	3.31363		0.00004
53	-2.324	3.728	4.186	3.27107		0.00004
54	-2.465	3.767	4.254	3.22812		0.00004
55	-2.608	3.806	4.32	3.18478		0.00004
56	-2.752	3.846	4.386	3.14107		0.00004
57	-2.896	3.887	4.45	3.09703		0.00003
58	-3.042	3.928	4.514	3.05271		0.00003
59	-3.188	3.97	4.577	3.00816		0.00003

m	x_m	$\Omega_m^{(1)}$	$\Omega_m^{(2)}$	$\left\|y_m^{(50)} - \Omega_m^{(1)}\right\|$		$\left\|y_m^{(50)} - \Omega_m^{(2)}\right\|$
60	-3.336	4.013	4.638	2.96343		0.00003
61	-3.484	4.056	4.699	2.91858		0.00003
62	-3.633	4.1	4.759	2.87366		0.00003
63	-3.783	4.144	4.819	2.82873		0.00003
64	-3.934	4.189	4.877	2.78384		0.00003
65	-4.086	4.234	4.935	2.73904		0.00003
66	-4.239	4.28	4.992	2.69437		0.00003
67	-4.392	4.326	5.048	2.64988		0.00003
68	-4.546	4.373	5.104	2.6056		0.00003
69	-4.701	4.42	5.159	2.56157		0.00003
70	-4.857	4.467	5.213	2.51782		0.00003
71	-5.014	4.515	5.267	2.47437		0.00003
72	-5.171	4.562	5.321	2.43126		0.00003
73	-5.329	4.61	5.373	2.3885		0.00003
74	-5.488	4.658	5.426	2.34611		0.00003
75	-5.647	4.706	5.477	2.3041		0.00003
76	-5.808	4.755	5.528	2.26249		0.00003
77	-5.969	4.803	5.579	2.22129		0.00003
78	-6.13	4.851	5.629	2.18051		0.00003
79	-6.293	4.899	5.679	2.14015		0.00003
80	-6.456	4.948	5.728	2.10022		0.00003
81	-6.619	4.996	5.777	2.06072		0.00003
82	-6.784	5.044	5.826	2.02166		0.00003
83	-6.948	5.092	5.874	1.98302		0.00003
84	-7.114	5.14	5.922	1.94482		0.00003
85	-7.28	5.188	5.969	1.90706		0.00003
86	-7.447	5.235	6.016	1.86972		0.00003
87	-7.615	5.283	6.062	1.83281		0.00002
88	-7.783	5.33	6.109	1.79632		0.00002
89	-7.952	5.377	6.154	1.76025		0.00002
90	-8.121	5.424	6.2	1.72459		0.00002
91	-8.291	5.471	6.245	1.68934		0.00002
92	-8.461	5.518	6.29	1.65449		0.00002
93	-8.633	5.564	6.334	1.62003		0.00002
94	-8.804	5.611	6.378	1.58597		0.00002
95	-8.977	5.657	6.422	1.55228		0.00002
96	-9.149	5.702	6.465	1.51897		0.00002
97	-9.323	5.748	6.508	1.48603		0.00002
98	-9.497	5.793	6.551	1.45345		0.00002
99	-9.671	5.838	6.593	1.42123		0.00002
100	-9.846	5.883	6.634	1.38934		0.00002

m	x_m	$\Omega_m^{(1)}$	$\Omega_m^{(2)}$	$\left|y_m^{(50)} - \Omega_m^{(1)}\right|$		$\left|y_m^{(50)} - \Omega_m^{(2)}\right|$	
101	-10.022	5.928	6.676	1.3578		0.00002	
102	-10.198	5.972	6.716	1.32659		0.00002	
103	-10.375	6.016	6.757	1.29571		0.00002	
104	-10.552	6.06	6.797	1.26514		0.00002	
105	-10.73	6.104	6.836	1.23488		0.00002	
106	-10.908	6.148	6.875	1.20492		0.00002	
107	-11.087	6.191	6.913	1.17525		0.00002	
108	-11.266	6.234	6.951	1.14588		0.00002	
109	-11.446	6.277	6.988	1.11678		0.00002	
110	-11.626	6.319	7.025	1.08795		0.00002	
111	-11.807	6.361	7.061	1.0594		0.00002	
112	-11.988	6.404	7.096	1.0311		0.00002	
113	-12.17	6.445	7.131	1.00305		0.00002	
114	-12.352	6.487	7.165	0.97524		0.00002	
115	-12.535	6.529	7.199	0.94768		0.00002	
116	-12.718	6.57	7.231	0.92035		0.00001	
117	-12.901	6.611	7.263	0.89324		0.00001	
118	-13.086	6.652	7.294	0.86635		0.00001	
119	-13.27	6.692	7.325	0.83967		0.00001	
120	-13.455	6.733	7.354	0.81319		0.00001	
121	-13.641	6.773	7.383	0.78692		0.00001	
122	-13.827	6.813	7.411	0.76084		0.00001	
123	-14.013	6.853	7.439	0.73494		0.00001	
124	-14.2	6.893	7.465	0.70923		0.00001	
125	-14.387	6.932	7.491	0.68369		0.00001	
126	-14.575	6.971	7.516	0.65832		0.00001	
127	-14.763	7.011	7.541	0.63311		0.00001	
128	-14.952	7.05	7.564	0.60806		0.00001	
129	-15.141	7.088	7.587	0.58316		0.00001	
130	-15.33	7.127	7.609	0.5584		0.00001	
131	-15.52	7.166	7.631	0.53379		0.00001	
132	-15.711	7.204	7.652	0.50932		0.00001	
133	-15.901	7.242	7.672	0.48497		0.00001	
134	-16.092	7.28	7.692	0.46075		0.00001	
135	-16.284	7.318	7.711	0.43666		0.00001	
136	-16.476	7.356	7.729	0.41268		0.00001	
137	-16.668	7.393	7.747	0.38881		0.00001	
138	-16.861	7.431	7.765	0.36505		0.00001	
139	-17.055	7.468	7.782	0.3414		0.00001	
140	-17.248	7.505	7.798	0.31784		0.00001	

m	x_m	$\Omega_m^{(1)}$	$\Omega_m^{(2)}$	$\left\lvert y_m^{(50)} - \Omega_m^{(1)} \right\rvert$	$\left\lvert y_m^{(50)} - \Omega_m^{(2)} \right\rvert$
141	-17.442	7.542	7.814	0.29439	0.00001
142	-17.637	7.579	7.83	0.27103	0.00001
143	-17.831	7.616	7.846	0.24776	0.00001
144	-18.027	7.652	7.861	0.22459	0.00001
145	-18.222	7.688	7.876	0.20151	0.
146	-18.418	7.725	7.89	0.17852	0.
147	-18.615	7.761	7.905	0.15563	0.
148	-18.811	7.796	7.919	0.13284	0.
149	-19.009	7.832	7.933	0.11015	0.
150	-19.206	7.867	7.946	0.08756	0.
151	-19.404	7.902	7.96	0.06509	0.
152	-19.602	7.937	7.972	0.0426	0.
153	-19.801	7.972	7.978	0.02027	0.

Table 5.2: Results of 51st Iteration

5.2 Future Work

In this thesis, the modified BEM (Muleshkov, 1988) was used for two-dimensional unconfined flow. In particular, a seepage with toe drain or horizontal exit was used. In the future, one could try to generalize what is done in this thesis to the case of an exit with arbitrary angle θ. Furthermore, discussion of different kinds of singularities could merit research. An interesting example would be singularities that occur on cusps. Alternatively, another avenue of future research could be applying the modified BEM to other areas of physics or engineering such as steady-state heat flow, electrostatics, or elasticity. The following subsections discuss possible further research.

When attempting to extend this work to other areas of hydrodynamics? there are some immediate difficulties. While the BEM has been applied to multiphase flow, unsteady flow, leaky aquifers, and anisotropic aquifers, as well as many other types of flow problems (Liggett and Liu, 1983), the modified BEM may not be applicable in these situations. In its current form, the modified BEM's main limitation is the need for a Laplace equation with the boundary conditions that allow the use of conformal mapping. This requirement limits the application of the modified BEM to flow

problems with a low Reynolds number and low flow velocity.

5.2.1   Treatment of Singularity at Point B'

The explanation of why Chantasiriwan's algorithm becomes unstable as the height seepage surface approaches zero could be the fact that the exit point becomes a singularity. In Figure 2.1, it can be seen that point B is a regular point. However, in Figure 2.11, point B' is now a singularity, since line segment $B'B''$ does not have the boundary condition $\dfrac{\partial \phi}{\partial n} = 0$. This means we may apply the same conformal mapping modifications as what was done with the other singularities in this thesis. The preliminary work of applying the modification to the elements around the singular point B' is discussed in the remainder of this subsection. We consider the infinite extension of the sides adjacent to point B' in Figure 2.11 preserving the local behavior. This is shown in Figure 5.7. The corresponding domain of the domain in Figure 5.7 in the complex potential plane is shown in Figure 5.8. Note that the shape and location of line $B'B'_3$ is unknown in Figure 5.8.
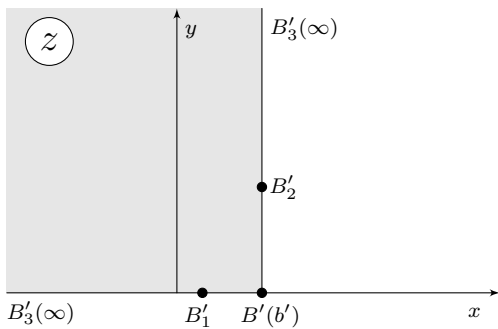

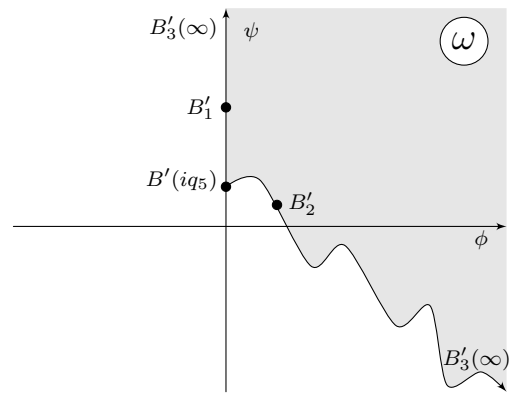Figure 5.7: Extension of Boundary Near Point B'

Figure 5.8: Domain in Complex Potential Plane of Figure 5.1

By using the complex velocity function $\dfrac{\mathrm{d}\omega}{\mathrm{d}z}$ and the intermediary domain in Fig 5.9 the conformal
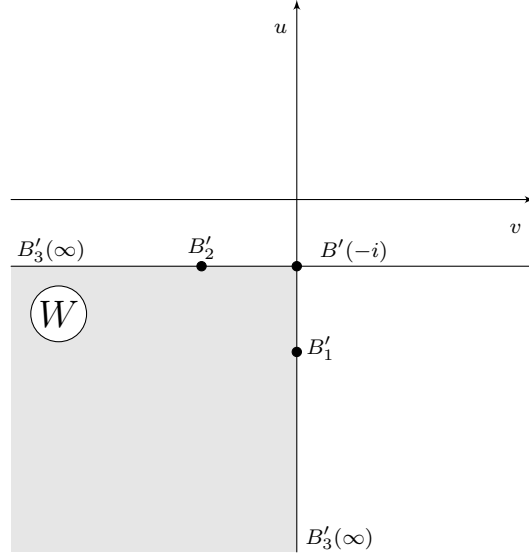
63

Figure 5.9: Domain in W-plane

mapping can be found.

The conformal mapping that maps the domain in Figure 5.7 to the corresponding domain Figure 5.8 is

$$\omega = iM_9\left(\frac{(z-b')^2}{2} - (z-b')\right) + iq_5 \tag{5.1}$$

where M_9 and q_5 are arbitrary real number. Since $\omega = \phi + i\psi$, $\phi(x,y)$ is the real part of ω. If we set $M_9 = 1$ and $q_5 = 0$. It can be shown that

$$\phi(x,y) = (1+b')y - xy \tag{5.2}$$

$$\psi(x,y) = \frac{1}{2}\left(b'^2 - 2b'(x-1) - 2x + x^2 - y^2\right) \tag{5.3}$$

is the solution of the BVP for the domain shown in Figure 5.7. Using Eqs.(5.2) and (5.3), Figure 5.10 is made. The figures do show that the behavior of the flow around B', where $b' = 1.5$ was used for the graphs, is concerning. Further work to treat the singularity, possibly leading to better results, can be done in the future.

64
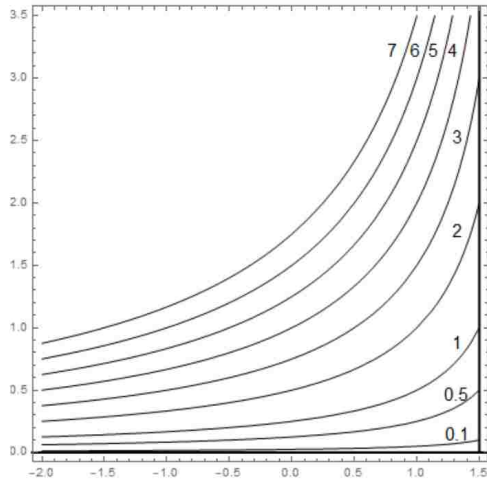
(a) Contour plot for various values of ϕ
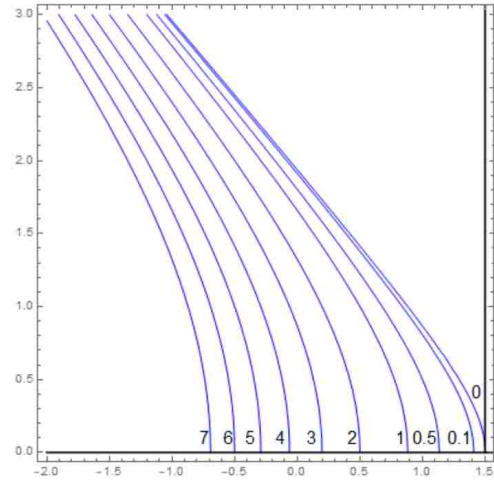
(b) Contour plot for various values of ψ
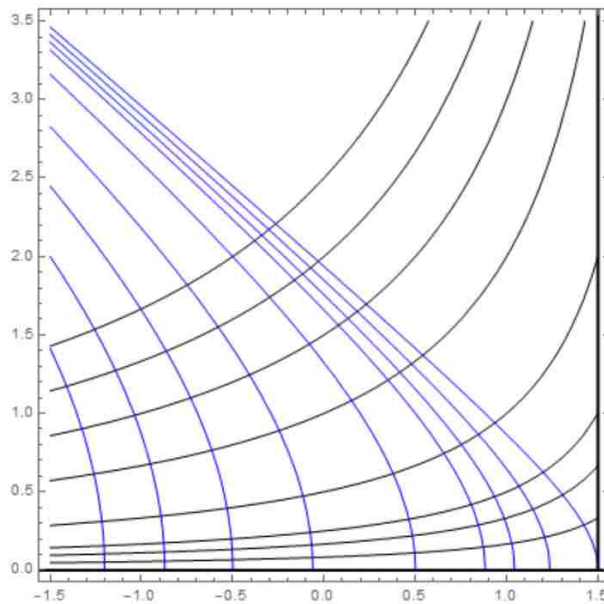
(c) Flownet of Figure 5.7

Figure 5.10: Contour Plots of Figure 5.7

5.2.2 Alternative Conformal Mappings Around Singular Points

The simplified domains used in the conformal mappings would be that they are not unique. To elaborate further, the style used in this thesis is not the only way to simplify a domain; one could use a simplified polygon or different infinite extensions. Another idea could be using more than 2 parts of the boundary. As an example of some of the ideas presented, Figure 5.11 illustrates a possible

alternative to what was done in Sections 4.3 and 4.4. This raises the question on whether under special circumstances if multiple singularities can be treated with the same conformal mapping.
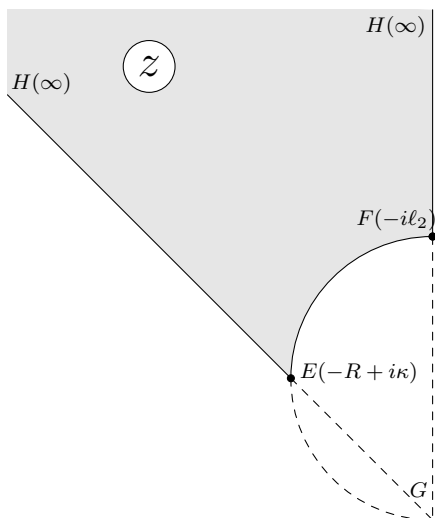

Figure 5.11: Extension of Boundary Near EF

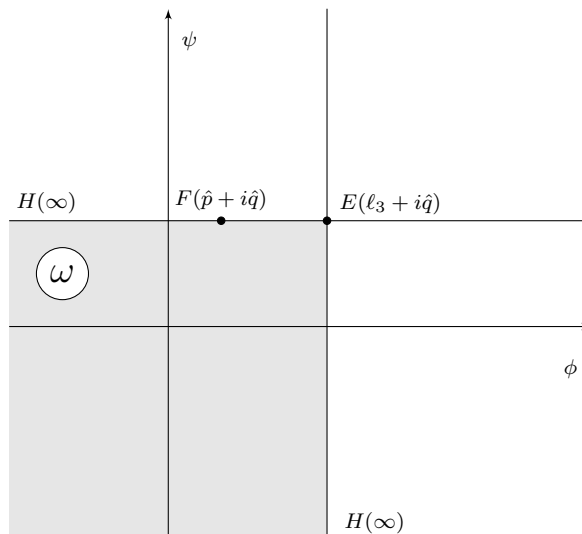Figure 5.12: Domain in Complex Potential Plane of Figure 5.11

The following conformal mapping would map the domain in Figure 5.11 to the right triangle in Figure 5.13.

$$Z_1(z) = \frac{z + (\kappa - R)i}{z + (\kappa + R)i} \tag{5.4}$$

The Domain in Figure 5.13 can then be mapped to the upper half plane using a Schwarz-Christoffel transformation, which for a triangle results in a Hypergeometric function.
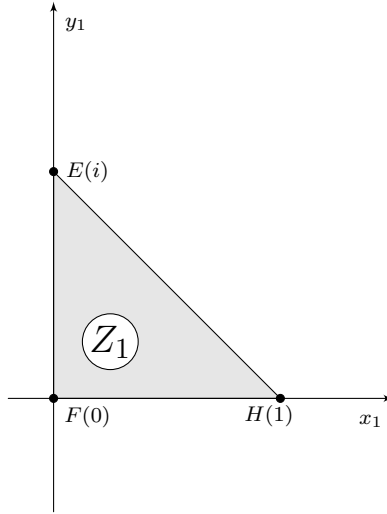
66

Figure 5.13: Domain in Z_1 Plane of the domain in Figure 5.11

5.2.3 Alternative Determination Algorithm for Locating the Phreatic Surface on Dams with Toe Drain

This thesis used the algorithm found in Chantasiriwan (2011) for location of the phreatic surface. As was discussed in subsection 5.2.1, this method is far from perfect. The inherent flaws of modifying the physical domain are clear. If one could find an alternative algorithm that does not depend on changing the domain of the BVP, that would be ideal. This can can be achieved by running the BEM algorithm multiple times, until either $\phi = 0$ or $\dfrac{\partial \phi}{\partial n} = 0$ at the exit point. Both methods seem promising and could be done using a method similar to the bisection method for finding zeros. However, this would be very inefficient, since each test would require the BEM to be performed on the boundary for every test. Nevertheless, the following figure shows the results of the first loop of these proposed algorithm.
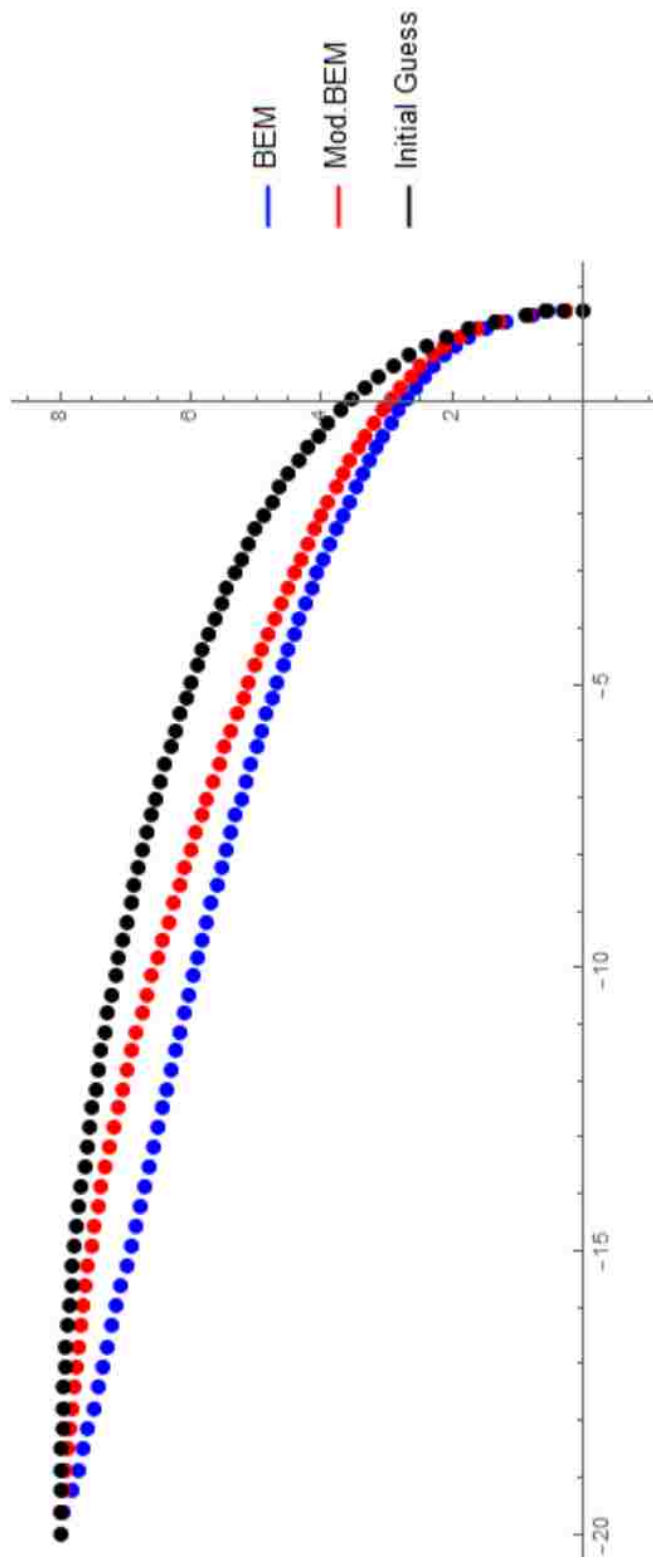
Figure 5.14: First Iteration of New Algorithm

Appendix A. List of Integrals Used and Their Solutions

Integral I_1

The Integral I_1 is given by

$$I_1(a, b, c, d) = \int_a^b \frac{b - z}{b - a} \ln \sqrt{(z - c)^2 + d^2} \, dz \tag{A.1}$$

where $a \neq b$ and $d \geq 0$.

I_1 is solved $\forall a, b, c, d \in \mathbb{R}$ in (Muleshkov, 1988). In the most general case, when $d > 0$, Eq.(A.1)

becomes

$$I_1(a, b, c, d) = \frac{(a - c)(a - 2b + c) + d^2}{2(b - a)} \ln \sqrt{(a - c)^2 + d^2} + \frac{1}{4}(a - 3b + 2c)$$
$$+ \frac{(b - c)^2 - d^2}{2(b - a)} \ln \sqrt{(b - c)^2 + d^2} + \frac{d(b - c)}{b - a} \left(\arctan \frac{b - c}{d} - \arctan \frac{a - c}{d} \right). \tag{A.2}$$

When $a \neq b \neq c$ and $d \to 0$ Eq.(A.2) becomes

$$I_1(a, b, c, 0) = \frac{(a - c)(a - 2b + c)}{2(b - a)} \ln |b - a| + \frac{(b - c)^2}{2(b - a)} \ln |b - c| + \frac{1}{4}(a - 3b + 2c). \tag{A.3}$$

When $c \to a$ and $d = 0$, Eq.(A.3) becomes

$$I_1(a, b, a, 0) = \frac{1}{2}(b - c) \ln |b - a| + \frac{3}{4}(a - b) \tag{A.4}$$

When $c \to b$ and $d = 0$, Eq.(A.3) becomes

$$I_1(a, b, b, 0) = \frac{1}{2}(b - a) \ln |b - a| + \frac{1}{4}(a - b) \tag{A.5}$$

Integral I_2

The Integral I_2 is given by

$$I_2(a, b, c, d) = \int_a^b \frac{b - z}{b - a} \cdot \frac{d}{(z - c)^2 + d^2} \, dz \tag{A.6}$$

where $a \neq b$.

I_2 is solved $\forall a, b, c, d \in \mathbb{R}$ in (Muleshkov, 1988). In the most general case, when $d \neq 0$, Eq.(A.6) becomes

$$I_2(a, b, c, d) = \frac{b - c}{b - a} \left(\arctan \frac{b - c}{d} - \arctan \frac{a - c}{d} \right) \frac{d}{b - a} \ln \sqrt{(b - c)^2 + d^2}$$

$$+ \frac{d}{b - a} \ln \sqrt{(a - c)^2 + d^2}. \tag{A.7}$$

When $d = 0$, Eq.(A.7) becomes

$$I_2(a, b, c, 0) = 0 \tag{A.8}$$

Integral I_3

The Integral I_3 is given by

$$I_3(a, b, c, d) = d \int_a^b \frac{dz}{(z - c)^2 + d^2} \tag{A.9}$$

where $a \neq b$.

I_3 is solved $\forall a, b, c, d \in \mathbb{R}$ in (Muleshkov, 1988). In the most general case, when $d \neq 0$, Eq.(A.9)

becomes

$$I_3(a, b, c, d) = \arctan \frac{b - c}{d} - \arctan \frac{a - c}{d} \tag{A.10}$$

When $d = 0$, from Eq.(A.28) becomes

$$I_3(a, b, c, 0) = 0 \tag{A.11}$$

Integral I_4

The Integral I_4 is given by

$$I_4(a, b, c) = \int_0^c \frac{z^3}{(z^3 - a)^2 + b^2} \, dz \tag{A.12}$$

where $c \neq 0$.

I_4 is solved for $b > 0$ in (Muleshkov, 1988) as $\widetilde{I_5}$. In the most general case, when $b > 0$, Eq.(A.12)

becomes

$$I_4(a, b, c) = \sum_{k=-1}^{1} \left[\frac{R_k}{2} \ln \left(1 - 2\mu_k \frac{c}{\lambda} + \frac{c^2}{\lambda^2} \right) + \frac{S_k}{\lambda \bar{\mu}_k} \left(\arctan \frac{\frac{c}{\lambda} - \mu_k}{\bar{\mu}_k} + \arctan \frac{\mu_k}{\bar{\mu}_k} \right) \right] \tag{A.13}$$

for $k \in \{-1, 0, 1\}$. Where

$$\lambda = \sqrt[6]{a^2 + b^2} \qquad\qquad \theta = \frac{1}{3} \arccos \frac{a}{\lambda^3}$$

$$\mu_k = \cos \left(\theta + \frac{2k\pi}{3} \right) \qquad\qquad \bar{\mu}_k = \sin \left(\theta + \frac{2k\pi}{3} \right)$$

$$R_k = \frac{\bar{\mu}_k}{3\lambda^2 \sin 3\theta} \qquad\qquad S_k = \frac{\mu_k \bar{\mu}_k}{3\lambda \sin 3\theta}.$$

71

Integral I_5

The Integral I_5 is given by

$$I_5(a, b, c) = \frac{3b}{c^4} \int_0^c \frac{z^6}{(z^3 - a)^2 + b^2} \, dz \tag{A.14}$$

where $c \neq 0$.

I_5 is solved $\forall a, b, c, d \in \mathbb{R}$ in (Muleshkov, 1988). In the most general case, when $b > 0$, Eq.(A.14)

becomes

$$I_5(a, b, c) = \frac{3b}{c^3} + \frac{\lambda^4}{c^4} \sum_{k=-1}^{1} \left[\bar{v}_k \ln \sqrt{1 - 2\mu_k \frac{c}{\lambda} + \frac{c^2}{\lambda^2}} + v_k \left(\arctan \frac{\frac{c}{\lambda} - \mu_k}{\bar{\mu}_k} + \arctan \frac{\mu_k}{\bar{\mu}_k} \right) \right] \tag{A.15}$$

Where

$$\lambda = \sqrt[6]{a^2 + b^2} \qquad\qquad \theta = \frac{1}{3} \arccos \frac{a}{\lambda^3}$$

$$\mu_k = \cos\left(\theta + \frac{2k\pi}{3}\right) \qquad\qquad \bar{\mu}_k = \sin\left(\theta + \frac{2k\pi}{3}\right)$$

$$v_k = \cos\left(4\theta + \frac{2k\pi}{3}\right) \qquad\qquad \bar{v}_k = \sin\left(4\theta + \frac{2k\pi}{3}\right)$$

for $k \in \{-1, 0, 1\}$. When $b \to 0$ but $a \neq c^3$, Eq.(A.15) becomes

$$I_5(a, 0, c) \to \frac{b}{c^4} \left(3c + \frac{ac}{a - c^3} + \frac{2\sqrt[3]{a}}{a - c^3} \ln \frac{(c - \sqrt[3]{a})^3}{c^3 - a} - \frac{4\sqrt[3]{a}}{\sqrt{3}} \left(\arctan\left(\frac{2c}{\sqrt{3}\sqrt[3]{a}} + \frac{1}{3} \right) - \frac{\pi}{6} \right) \right) \tag{A.16}$$

Also, when $a \to c^3$, Eq.(A.16) becomes

$$I_5(c^3, 0, c) = 0 \tag{A.17}$$

Integral I_6

The Integral I_6 is given by

$$I_6(a, b, c) = \frac{3}{2c} \int_0^c z^3 \ln\left[(z^3 - a)^2 + b^2\right] \, dz \tag{A.18}$$

Where $a \neq b$ and $b \geq 0$. I_6 is solved $\forall a, b, c, d \in \mathbb{R}$ in (Muleshkov, 1988). In the most general case, when $b > 0$, Eq.(A.18) becomes

$$I_6(a, b, c) = \frac{3c^3}{8} \ln\left((c^3 - a)^2 + b^2\right) - \frac{9}{16}c^3 - \frac{9}{4}a + \frac{3}{4c}\lambda^4 \sum_{k=-1}^{1} \left[-v_k \ln\sqrt{1 - 2\mu_k \frac{c}{\lambda} + \frac{c^2}{\lambda^2}} \right.$$
$$\left. + \bar{v}_k \left(\arctan\frac{\frac{c}{\lambda} - \mu_k}{\bar{\mu}_k} + \arctan\frac{\mu_k}{\bar{\mu}_k} \right) \right] \tag{A.19}$$

Where

$$\lambda = \sqrt[6]{a^2 + b^2} \qquad\qquad \theta = \frac{1}{3} \arccos\frac{a}{\lambda^3}$$

$$\mu_k = \cos\left(\theta + \frac{2k\pi}{3}\right) \qquad\qquad \bar{\mu}_k = \sin\left(\theta + \frac{2k\pi}{3}\right)$$

$$v_k = \cos\left(4\theta + \frac{2k\pi}{3}\right) \qquad\qquad \bar{v}_k = \sin\left(4\theta + \frac{2k\pi}{3}\right).$$

When $b \to 0$, Eq.(A.19) becomes

$$I_6(a, 0, c) = \frac{3}{4}c^3 \ln|c^3 - a| - \frac{9}{16}c^3 - \frac{9}{4}a - \frac{3}{4c}\sqrt[3]{a^4} \ln\left|\frac{c}{\sqrt[3]{a}} - 1\right| +$$
$$\frac{3}{8c}\sqrt[3]{a^4} \ln\left|1 + \frac{c}{\sqrt[3]{a}} + \frac{c^2}{\sqrt[3]{a^2}}\right| + \frac{3\sqrt{3}}{4c}\sqrt[3]{a^4} \arctan\left(\frac{1}{\sqrt{3}} + \frac{2c}{\sqrt{3}\sqrt[3]{a}}\right) - \frac{\sqrt{3}\pi}{8}\sqrt[3]{a^4} \tag{A.20}$$

Also, when $c \to \sqrt[3]{a}$, Eq.(A.20) becomes

$$I_6(a, 0, \sqrt[3]{a}) = \frac{9}{8}c^3 \left(\ln c^2 + \ln 3 - \frac{5}{2} + \frac{\pi}{3\sqrt{3}} \right) \tag{A.21}$$

Integral I_7

The Integral I_7 is given by

$$I_7(a, b, c, d, f) = \int_a^b \left(\frac{b-z}{b-a}\right) \frac{f^2 - cf\cos(z) - df\sin(z)}{(f\cos(z) - c)^2 + (f\sin(z) - d)^2} \, dz \qquad \text{(A.22)}$$

where $a \neq b$ and $f > 0$.

I_7 is solved numerically using Mathematica (Wolfram Research Inc. 2018).

Integral I_8

The Integral I_8 is given by

$$I_8(a, b, c, d) = \frac{1}{\zeta} \int_a^b \left(\frac{\partial\phi}{\partial x}(z, -z - \ell_2 - 2R) + \frac{\partial\phi}{\partial y}(z, -z - \ell_2 - 2R)\right) \ln\left(\sqrt{2}\sqrt{(z-c)^2 + d^2}\right) dz$$

$$\text{(A.23)}$$

Where $a \neq b$.

I_8 is solved numerically using Mathematica (Wolfram Research Inc. 2018).

Integral I_9

The Integral I_9 is given by

$$I_9(a, b, c, d, f) = \int_a^b \left(\hat{f}(z)\hat{g}(z)\right) \frac{f^2 - cf\cos(z) - df\sin(z)}{(f\cos(z) - c)^2 + (f\sin(z) - d)^2} \, dz \qquad \text{(A.24)}$$

where $a \neq b$.

I_9 is solved numerically using Mathematica (Wolfram Research Inc. 2018).

Integral I_{10}

The Integral I_{10} is given by

$$I_{10}(a, b, c, d, f) = \int_a^b \left(1 - \frac{\hat{f}(z)\hat{g}(z)}{\hat{f}(\theta_{K_4+2})\hat{g}(\theta_{K_4+2})} \right) \frac{f^2 - cf\cos(z) - df\sin(z)}{(f\cos(z) - c)^2 + (f\sin(z) - d)^2} \, dz \qquad \text{(A.25)}$$

where $a \neq b$.

I_{10} is solved numerically using Mathematica (Wolfram Research Inc. 2018).

Integral I_{11}

The Integral I_{11} is given by

$$I_{11}(a, b, c, d, f, g) = \int_a^b \left(g - \sin\theta_{K_5-1} \right) \frac{f^2 - cf\cos(z) - df\sin(z)}{(f\cos(z) - c)^2 + (f\sin(z) - d)^2} \, dz \qquad \text{(A.26)}$$

where $a \neq b$.

I_{11} is solved numerically using Mathematica (Wolfram Research Inc. 2018).

Integral I_{12}

The Integral I_{12} is given by

$$I_{12}(a, b, c, d, f) = \int_a^b \frac{d}{(f - z)((z - c)^2 + (d)^2)} \, dz \qquad \text{(A.27)}$$

where $a \neq b$.

I_{12} is solved $\forall a, b, c, d, f \in \mathbb{R}$. In the most general case, when $d \neq 0$, Eq.(A.27) becomes

$$I_{12}(a, b, c, d, f) = \frac{1}{2(d^2 + (c - f)^2)}\left(2(c - f)\left(\arctan\left(\frac{a - c}{d}\right) - \arctan\left(\frac{b - c}{d}\right)\right)\right.$$
$$\left. + d\left(\log\left|\frac{(b - c)^2 + d^2}{(a - c)^2 + d^2}\right| + 2\log\left|\frac{a - f}{b - f}\right|\right)\right) \quad \text{(A.28)}$$

When $d = 0$, from Eq.(A.27) becomes

$$I_{12}(a, b, c, 0, f) = 0 \quad \text{(A.29)}$$

BIBLIOGRAPHY

Bear, Jacob. 1972. *Dynamics of Fluids in Pororus Media*, American Elsevier, New York, NY.

———. 2018. *Modeling Phenomena of Flow and Transport in Porous Media*, Theory and Application of Transport in Porous Media, Springer, Cham.

Bruch, Erwin K. 1991. *The Boundary Element Method for Groundwater Flow*, 70th ed. (C.A. Brebbia and S.A. Orszag, eds.), Lecture Notes in Engineering, Springer-Verlag, Berlin.

Carrier, George F., Max Krook, and Carl E. Pearson. 1983. *functions of a complex variable*: *theory and technique*, Hod Books,Ithaca, NY.

Cedergen, Harry R. 1968. *Seepage, Drainage, and Flow Nets*, John Wiley & Sons, inc. , New York.

Chantasiriwan, Somchart. 2011. *Determination of Free Surface in Steady-State Seepage through a Dam with Toe Drain by the Boundary Element Method*, Science & Technology Asia **16**, no. 4, 1-7. https://www.tci-thaijo.org/index.php/SciTechAsia/article/view/41197.

Chen, Jeng-Tzong, Chia-Chun Hsiao, Yi-Ping Chiu, and Ying-Te Lee. 2007. *Study of Free-Surface Seepage Problem using Hypersingular equations*, Communications in Numerical Methods in Engineering **23**.

Evans, Lawrence C. 2010. *Partial Differential Equations*, 2nd, Graduate Studies in Mathematics, vol. 19, American Mathematical Society.

Harr, Martin E. 1962. *Groundwater and Seepage*, McGraw-Hill, New York.

Igarashi, Hajime and Toshihisa Honma. 1996. *A Boundary Element Method for Potential Fields with Corner Singularitites*, Applied Mathematical Modeling **20**.

Kythe, Prem K. 1995. *An Introduction to the Boundary Element Method*, CRC Press, Boca Raton, Florida.

Lacy, Sara J. and Jean H. Prevost. 1987. *Flow Through Porous Media: A Procedure for Locating the Free Surface*, International Journal For Numerical and Analytical Method in Geomechanics **11**.

Layton, William J. 2008. *Introduction to the Numerical Analysis of Incompressible Viscous Flows*, Computational Science & Engineering, vol. 6, Siam, Philadelphia, PA.

Lefeber, Dirk. 1989. *Solving problems with singularities using boundary method*, Topics in engineering, Computational Mechanics, Boston.

Liggett, James A. and Philip L-F. Liu. 1983. *The Boundary Integral Equation Method for Porous Media Flow*, George Allen & Unwin, London.

Mathews, John H. and Russell W. Howell. 2012. *Complex Analysis*: *For Mathematics and Engineering*, Sixth, Jones & Bartlett learning,.

Muleshkov, Angel. 1988. *Analytical and Boundary Element Solutions of Steady Seepage Towards Vertical Cuts*, University of Washington.

———. 2016. *Lectures on Conformal Mapping. Mat 709-710*. Personal Collection of A. Muleshkov, University of Nevada Las Vegas, Las Vegas, NV.

Romero, Megan. 2018. *Conformal mapping improvement of the boundary element method solution for underground water flow in a domain with a very singular boundary*, University of Nevada Las Vegas. Masters Thesis.

Tice, Ian. 2014. *From Stokes Flow To Darcy's Law*. Center for Nonlinear Analysis lecture notes.

Wang, Hui, Ya-Ting Gao, and Qing-Hua Qin. 2015. *Green's function based finite element formulation for isotropic seepage analysis with free surface*, Latin American Journal of Solid and Structures.

Wolfram Research Inc. 2018. *Mathematica 11*, Wolfram Research Inc. ,Champaign , IL.

Yeung, Ronald W. 1982. *Numerical Methods in Free-Surface Flows*, Annual Reviews Fluid Mechanics.

CURRICULUM VITAE

Graduate College

University of Nevada, Las Vegas

Jorge Eduardo Reyes Jr.

Email:

    `reyesejorge.jr@gmail.com`

Degrees:

    Bachelor of Science, Mathematics, 2015
    University of Nevada, Las Vegas

    Associate of General Studies, 2014
    College of Southern Nevada, Las Vegas

Thesis Title: An Application of Conformal Mapping to the Boundary Element Method for Steady Seepage with a Phreatic Surface

Thesis Examination Committee:

    Chairperson, Dr. Angel S. Muleshkov, Ph.D.

    Committee Member, Dr. Monika Neda, Ph.D.

    Committee Member, Dr. Pengtao Sun, Ph.D.

    Graduate Faculty Representative, Dr. David D. Kreamer, Ph.D.